

1 **A STABLE MATRIX VERSION OF THE FAST MULTIPOLE METHOD:**
 2 **STABILIZATION STRATEGIES AND EXAMPLES***

3 DIFENG CAI[†] AND JIANLIN XIA[‡]

4 **Abstract.** The fast multipole method (FMM) is an efficient method for evaluating matrix-vector products related
 5 to certain discretized kernel functions. The method involves an underlying FMM matrix given by a sequence of
 6 smaller matrices (called generators for convenience). Although there have been extensive work in designing and
 7 applying FMM techniques, the stability of the FMM and the stable FMM matrix factorization have rarely been studied.
 8 In this work, we propose techniques that lead to stable operations with FMM matrices. One key objective is to give
 9 stabilization strategies that can be used to provide low-rank approximations and translation relations in the FMM
 10 satisfying some stability requirements. Standard Taylor expansions used in FMM methods yield basis generators
 11 susceptible to instability. Here, we introduce some scaling factors to control relevant norms of the generators and give
 12 rigorous analysis on the bounds of entrywise magnitudes. The second objective is to use the one-dimensional case as
 13 an example to show an intuitive construction of FMM matrices satisfying some stability conditions and then convert
 14 an FMM matrix into a hierarchically semiseparable (HSS) form that admits stable ULV-type factorizations. This
 15 bridges the gap between the FMM and stable FMM matrix factorizations. The HSS construction is done analytically
 16 and does not need expensive algebraic compression. Relevant stability studies are given and show that the resulting
 17 matrix forms are suitable for stable operations. Note that the essential stabilization ideas are also applicable to higher
 18 dimensions. Extensive numerical tests are given to illustrate the reliability and accuracy.

19 **Key words.** numerical stability, fast multipole method, FMM matrix, scaling factor, low-rank approximation,
 20 HSS matrix

21 **AMS subject classifications.** 65F30, 65F35, 15A23, 15A60

22 **1. Introduction.** Let $\kappa(x, y)$ be a kernel function in a form such as $1/(x-y)$, $1/(x-y)^2$,
 23 $\log(x-y)$, and $\log|x-y|$, where $x, y \in \mathbb{C}$, $x \neq y$. Given a set of points

$$(1.1) \quad \mathbf{s} \equiv \{x_1, \dots, x_n\}, \quad x_i \in \mathbb{C},$$

24 let A be an $n \times n$ discretized matrix with entries

$$(1.2) \quad A_{ij} = \kappa(x_i, x_j), \quad i \neq j.$$

25 (The diagonal entries A_{ii} are defined separately and do not concern us so far.) It is well known
 26 that the fast multipole method (FMM) [16, 29] can be used to evaluate the product of A with
 27 a vector to a given accuracy in linear complexity. As shown in [32], the FMM essentially
 28 yields a hierarchical structured approximation to A to a given accuracy. Such a structured
 29 approximation is also an example of an \mathcal{H}^2 -matrix [18, 20]. For convenience, we refer to this
 30 approximation derived with the FMM procedure as an *FMM matrix*.

31 The construction of an FMM matrix often involves appropriate degenerate approximations
 32 or truncated expansions of $\kappa(x, y)$. Commonly used expansions are Taylor expansions,
 33 multipole expansions, and spherical harmonic expansions. Such expansions provide convenient
 34 ways to obtain low-rank approximations of off-diagonal blocks $(\kappa(x_i, y_j))_{x_i \in \mathbf{x}_1, y_j \in \mathbf{x}_2}$ of A
 35 that correspond to well-separated subsets \mathbf{x}_1 and \mathbf{x}_2 of \mathbf{s} . (This will be made more precise
 36 later.)

37 Practical implementations of the FMM have usually been very successful in achieving
 38 both high efficiency and nice accuracy. On the other hand, it has also been noticed that
 39 numerical stability issues may arise under certain circumstances [10, 11, 12, 17, 28]. Here in
 40 particular, we are interested in the stability of the FMM based on Taylor expansions of $\kappa(x, y)$.

*The research of Jianlin Xia was supported in part by an NSF grant DMS-1819166.

†Department of Mathematics, Emory University, Atlanta, GA 30322, USA (difeng.cai@emory.edu).

‡Department of Mathematics, Purdue University, West Lafayette, IN 47907, USA (xiaj@purdue.edu).

41 Taylor expansions can produce low-rank basis matrices with very large entries, although
 42 the original matrix entries $\kappa(x_i, y_j)$ may only have modest magnitudes. Examples of such
 43 terms are factorials and powers. The artificially large terms may lead to stability issues in
 44 relevant matrix operations, as pointed out in [17]. They can cause loss of accuracy (due to the
 45 magnification of numerical errors) or even overflow. Note that these stability risks can arise
 46 even if $\kappa(x, y)$ is non-oscillatory as considered here. This happens especially when the data
 47 points are not nicely distributed, like in the case in [28] where accuracy is crucial when dealing
 48 with data points that are clustered eigenvalues. Thus, it is important to study the relevant
 49 numerical stability. A heuristic strategy to improve the stability is briefly mentioned in [17],
 50 but is lack of rigorous justification or guarantee of the performance. (Note that, despite the
 51 stability risks, the FMM has worked well for many different problems, likely due to the use of
 52 certain basis or translation operators that have some structures or sparsity.)

53 Here, for the FMM based on Taylor expansions, our first objective is to provide a stabili-
 54 lization strategy by analytically obtaining low-rank basis matrices and translation matrices
 55 that satisfy some stability requirements. More specifically, we design a scaling strategy where
 56 some appropriate scaling factors are chosen to modify the individual terms in the Taylor ex-
 57 pansions. Then for well-separated subsets $\mathbf{x}_1, \mathbf{x}_2 \subset \mathbf{s}$, the block $(\kappa(x_i, y_j))_{x_i \in \mathbf{x}_1, y_j \in \mathbf{x}_2}$ can
 58 be approximated by a low-rank form $\hat{U} \hat{B} \hat{V}^T$, where the entries of \hat{U} and \hat{V} have magnitudes
 59 bounded by 1 and, moreover, the entries of \hat{B} have magnitudes bounded by a small multiple
 60 of $|\kappa(x, y)|$ evaluated at appropriate centers of \mathbf{x}_1 and \mathbf{x}_2 . See Theorem 2.5 for details. The
 61 low-rank approximations in the FMM also involve the key concept of a translation matrix. We
 62 give one specific form of the translation matrix and further show that, after scaling with our
 63 scaling factors, the entries of the translation matrix also have entrywise magnitudes bounded
 64 by 1. See Theorem 2.7. Based on these bounds, the stability of matrix operations with the
 65 resulting structured forms can be naturally shown. We illustrate a basic idea of the backward
 66 stability analysis in Theorem 2.9.

67 Our second objective is to extend the stabilization to another structured matrix form
 68 so as to bridge the gap between the FMM and stable direct factorizations. We use the one-
 69 dimensional (1D) case as an example to provide an intuitive way to write an explicit form of
 70 the FMM matrix based on the stabilization strategies. Then the 1D FMM matrix is converted
 71 into a hierarchical semiseparable (HSS) form [5, 7, 38] that is frequently used to design
 72 structured direct solvers. The 1D case is very useful for computations such as such as PDE
 73 solutions, Toeplitz solutions, polynomial computations, and eigenvalue solutions. See, e.g.,
 74 [5, 8, 13, 25, 26, 31, 33]. The original FMM [16] explains the method in terms of potential
 75 evaluations. Here, we show a stable matrix version that can be conveniently understood based
 76 on appropriate basis matrices as *contributions*, organized at different hierarchical levels by
 77 a nested basis relation. This matrix form is convenient for non-experts to grasp the FMM.
 78 An FMM matrix $\hat{A} \approx A$ is given in terms of a sequence of smaller matrices (which we call
 79 FMM generators) such as $\hat{U}, \hat{B}, \hat{V}$ as above and some translation matrices. \hat{A} enables fast
 80 matrix-vector multiplications, but the stable factorization has been unknown. By converting \hat{A}
 81 into an HSS form, we can take advantage of many fast and stable HSS algorithms, especially
 82 the so-called HSS ULV factorization [7] with proven nice backward stability [34, 35]. The
 83 FMM to HSS conversion is done analytically and avoids explicit algebraic compression like
 84 expensive truncated SVDs or randomized sampling used in [23, 24, 30, 38, 39]. The resulting
 85 HSS form is represented by a sequence of so-called HSS generators and can be factorized in
 86 $\mathcal{O}(n)$ complexity. All the FMM and HSS generators satisfy some norm bounds (see Corollary
 87 3.4) that can be used to show the stability of FMM and HSS algorithms. The techniques can
 88 also be generalized to the 2D case.

89 Overall, this work provides useful stability safeguards for matrix operations using the
 90 FMM matrices. We show how and why the stabilization works and illustrate some essential

91 ideas for the relevant backward stability analysis. We further give an example to illustrate
 92 an intuitive matrix version of the stable FMM. An analytical construction of HSS matrices
 93 from FMM matrices is also given so as to facilitate stable direct ULV factorizations. Our
 94 stabilization strategies are derived in terms of 2D point sets. We would like to emphasize
 95 that *the stabilization strategies and the stability studies are not restricted to 2D cases and are*
 96 *also applicable to higher dimensions*. Also, the use of the 1D example to illustrate the FMM
 97 matrix form is merely for convenience. The stabilization can also be applied to several kernel
 98 functions with related Taylor series expansions.

99 The structure of the paper is as follows. Section 2 shows the ideas of stabilizing the FMM
 100 via stable analytical low-rank approximations and translation operations. In Section 3, the
 101 ideas are then used for the construction of the FMM matrix, which is further converted into an
 102 HSS matrix. Some discussions and extensive numerical tests are given in Section 4 to illustrate
 103 the stability and accuracy.

104 **2. Stabilization of the FMM: stable low-rank approximation and translation operation.** In this section, we show how to obtain low-rank kernel matrix approximations that are
 105 suitable for stable operations. We further provide a stable translation relation to derive nested
 106 basis matrices. The techniques give essential components for stabilizing the FMM.
 107

108 **2.1. Kernel expansions and low-rank kernel matrix approximations.** Suppose a ker-
 109 nel function $\kappa(x, y)$ has a degenerate approximation of the following form for some x, y
 110 points:

$$(2.1) \quad \kappa(x, y) \approx \sum_{k=0}^{r-1} \sum_{l=0}^k \alpha_{k,l} \phi_l(x) \psi_{k-l}(y).$$

111 We suppose the points are from 2D point sets and are treated as complex numbers. (This can be
 112 modified to accommodate higher dimensions.) It is well-known that, if r is small compared to
 113 the numbers of x, y points, (2.1) yields a low-rank approximation to the kernel matrix (defined
 114 by the evaluation of $\kappa(x, y)$ at those x, y points). Here for simplicity, we mainly illustrate our
 115 techniques in terms of the following kernel:

$$(2.2) \quad \kappa(x, y) = \frac{1}{x - y}, \quad x \neq y.$$

116 Note that *the use of this kernel is only for convenience since the ideas can be immediately*
 117 *extended to several other kernels with similar degenerate approximations (see Section 2.4*
 118 *below)*. For such kernels, Taylor expansions can be used to obtain (2.1).

119 We show some details of the expansion following a strategy in [32] so as to facilitate our
 120 later derivations. For a set of points $\mathbf{x} \subset \mathbb{C}$, a point $z \in \mathbb{C}$ is said to be a center for \mathbf{x} with a
 121 corresponding radius if $|x - z| \leq \delta$ for any $x \in \mathbf{x}$. Such a definition for z and δ is used in
 122 [32] and some other FMM work. It is clear that z and δ may not be unique. In case unique z
 123 and δ are to be defined, we may use a disk enclosing the points with the smallest radius. Since
 124 the uniqueness is not a concern here, we simply follow the tradition in [32]. The following
 125 definition from [32] is a generalization of the classical definition of well-separated sets.

126 **DEFINITION 2.1.** [32] Suppose \mathbf{x}_1 and \mathbf{x}_2 are two sets of points in \mathbb{C} respectively
 127 corresponding to centers $z_1 \in \mathbb{C}$ and $z_2 \in \mathbb{C}$ and radii $\delta_1 > 0$ and $\delta_2 > 0$. \mathbf{x}_1 and \mathbf{x}_2 are said
 128 to be (well) separated (with separation ratio τ) if the following admissibility condition holds:

$$(2.3) \quad \delta_1 + \delta_2 \leq \tau |z_1 - z_2|, \quad \tau \in (0, 1).$$

129 For two well-separated sets $\mathbf{x}_1, \mathbf{x}_2 \subset \mathbf{s}$ as in Definition 2.1 with \mathbf{s} in (1.1), (2.3) implies,
 130 for any $x \in \mathbf{x}_1$ and $y \in \mathbf{x}_2$,

$$(2.4) \quad \left| \frac{(x - z_1) - (y - z_2)}{z_2 - z_1} \right| \leq \frac{\delta_1 + \delta_2}{|z_2 - z_1|} \leq \tau.$$

Applying Taylor expansion leads to

$$(2.5) \quad \begin{aligned} \kappa(x, y) &= -\frac{1}{(z_2 - z_1)[1 - \frac{(x - z_1) - (y - z_2)}{z_2 - z_1}]} \\ &= -\frac{1}{z_2 - z_1} \sum_{k=0}^{r-1} \left[\frac{(x - z_1) - (y - z_2)}{z_2 - z_1} \right]^k + \epsilon_r \\ &= -\sum_{k=0}^{r-1} \frac{k!}{(z_2 - z_1)^{k+1}} \sum_{j=0}^k (-1)^{k-j} \frac{(x - z_1)^j}{j!} \frac{(y - z_2)^{k-j}}{(k-j)!} + \epsilon_r \\ &= \sum_{k=0}^{r-1} \alpha_k \sum_{j=0}^k (-1)^{k-j} f_j(x - z_1) f_{k-j}(y - z_2) + \epsilon_r, \end{aligned}$$

131 where

$$(2.6) \quad f_j(x) = \frac{x^j}{j!}, \quad \alpha_k = -\frac{k!}{(z_2 - z_1)^{k+1}}, \quad |\epsilon_r| \leq \frac{\tau^r}{|z_2 - z_1|(1 - \tau)}.$$

Note that, by (2.4),

$$(2.7) \quad \begin{aligned} |\kappa(x, y)| &\geq \frac{1}{|(x - z_1) - (y - z_2)| + |z_1 - z_2|} \\ &\geq \frac{1}{\tau|z_1 - z_2| + |z_1 - z_2|} = \frac{1}{1 + \tau} |\kappa(z_1, z_2)|. \end{aligned}$$

132 Hence, the truncation error ϵ_r can be estimated by

$$|\epsilon_r| \leq \frac{\tau^r}{1 - \tau} |\kappa(z_1, z_2)| \leq \tau^r \frac{1 + \tau}{1 - \tau} |\kappa(x, y)|,$$

133 which indicates that the relative error of approximation (2.5) is bounded by $\tau^r \frac{1 + \tau}{1 - \tau}$. This is
 134 consistent with a conclusion in [32].

135 According to (2.5) and (2.6), we can then write

$$(2.8) \quad \kappa(x, y) = u^T \bar{B} v + \epsilon_r,$$

where

$$(2.9) \quad \begin{aligned} u &= [f_0(x - z_1) \quad f_1(x - z_1) \quad \cdots \quad f_{r-1}(x - z_1)]^T, \\ v &= [f_0(y - z_2) \quad f_1(y - z_2) \quad \cdots \quad f_{r-1}(y - z_2)]^T, \\ \bar{B} &= \begin{bmatrix} \alpha_0 & \alpha_1 & \cdots & \alpha_{r-1} \\ \alpha_1 & \ddots & \ddots & \\ \vdots & \ddots & & \\ \alpha_{r-1} & & & 0 \end{bmatrix} \text{diag}((-1)^0, (-1)^1, \dots, (-1)^{r-1}). \end{aligned}$$

136 Here, $\text{diag}(\dots)$ is used to represent a diagonal matrix (or a block diagonal matrix later).
 137 Then we consider the low-rank approximation of the discretized matrix defined by the
 138 evaluation of $\kappa(x, y)$ on $\mathbf{x}_1, \mathbf{x}_2$:

$$(2.10) \quad K = (\kappa(x_i, x_j))_{x_i \in \mathbf{x}_1, x_j \in \mathbf{x}_2},$$

139 which has the (i, j) entry $\kappa(x_i, y_j)$. K is $m \times p$ with $m = |\mathbf{x}_1|$, $p = |\mathbf{x}_2|$, and is sometimes
 140 referred to as the *interaction* (matrix) between \mathbf{x}_1 and \mathbf{x}_2 . Based on (2.8), K has a low-rank
 141 approximation

$$(2.11) \quad K = \bar{U} \bar{B} \bar{V}^T + K \odot E \approx \bar{U} \bar{B} \bar{V}^T,$$

where \odot denotes the entrywise (Hadamard) product and

$$(2.12) \quad \bar{U} = (f_{j-1}(x_i - z_1))_{m \times r}, \quad \bar{V} = (f_{j-1}(y_i - z_2))_{p \times r},$$

$$(2.13) \quad |E_{ij}| \leq \tau^r \frac{1 + \tau}{1 - \tau}.$$

142 (Here, notation like $(A_{ij})_{m \times n}$ means an $m \times n$ matrix with the (i, j) entry A_{ij} .) We see that
 143 \bar{U} and \bar{V} are fully determined by the sets \mathbf{x}_1 and \mathbf{x}_2 , respectively. The matrix \bar{B} is an $r \times r$
 144 matrix that depends only on $z_2 - z_1$.

145 **2.2. Stable low-rank approximation with scaling factors and analysis of entrywise**
 146 **magnitudes.** According to (2.9) and (2.12), the matrices $\bar{U}, \bar{B}, \bar{V}$ in the low-rank approxima-
 147 tion (2.11) may have large entrywise magnitudes. This is because of the powers and factorials
 148 in (2.6). As mentioned in the introduction, directly using the forms of $\bar{U}, \bar{B}, \bar{V}$ may cause
 149 stability issues in the low-rank approximation (2.11) and later operations. The stability issue
 150 gets more severe when r or the size of K increases. To ensure numerical stability, we introduce
 151 a scaling strategy so as to bound the entries of the factors in the low-rank approximation. We
 152 further rigorously justify the effectiveness of the scaling.

153 One set of scaling parameters is used for each set of points $\mathbf{x}_i \subset \mathbf{s}$ for \mathbf{s} in (1.1). Suppose
 154 \mathbf{x}_i has center z_i and radius δ_i . (Here, we use subscripts in bold fonts to denote indices of point
 155 sets.) For a set \mathbf{x}_i , define *scaling factors*

$$(2.14) \quad \eta_{i,j} = \begin{cases} 1, & j = 0, \\ \left(\frac{j}{e}(2\pi r)^{\frac{1}{2r}} \frac{1}{\delta_i}\right)^j, & j = 1, 2, \dots, r-1. \end{cases}$$

156 (We would like to point out that we first showed these scaling factors $\eta_{i,j}$ in our earlier
 157 unsubmitted preprint [4]. Later, the paper [3] briefly mentioned $\eta_{i,j}$ by citing [4].) Such a
 158 form is motivated by Stirling's formula:

$$\lim_{r \rightarrow \infty} \frac{r!}{\sqrt{2\pi r} (r/e)^r} = 1, \quad \text{or} \quad r! \sim \sqrt{2\pi r} \left(\frac{r}{e}\right)^r \text{ for large } r.$$

159 We use $\eta_{i,j}$ to modify the approximation to K in (2.10) with two separated sets \mathbf{x}_1 and \mathbf{x}_2 .
 160 For $x \in \mathbf{x}_1$ and $y \in \mathbf{x}_2$, the expansion in (2.5) can be rewritten as

$$(2.15) \quad \kappa(x, y) = \sum_{k=0}^{r-1} \alpha_k \sum_{j=0}^k (-1)^{k-j} (\eta_{1,j})^{-1} (\eta_{2,k-j})^{-1} (\eta_{1,j} f_j(x - z_1)) (\eta_{2,k-j} f_{k-j}(y - z_2)) + \epsilon_r.$$

161 Compared with (2.11), the approximation to K now becomes

$$(2.16) \quad K = \hat{U} \hat{B} \hat{V}^T + K \odot E \approx \hat{U} \hat{B} \hat{V}^T,$$

162 where

$$(2.17) \quad \begin{aligned} \hat{U} &= (\eta_{1,j-1} f_j(x_i - z_1))_{m \times r} \equiv \bar{U} S_1, \\ \hat{V} &= (\eta_{2,j-1} f_j(y_i - z_2))_{p \times r} \equiv \bar{V} S_2, \\ \hat{B} &= S_1^{-1} \bar{B} S_2^{-1}, \end{aligned}$$

163 and for $\mathbf{i} = 1, 2$,

$$(2.18) \quad S_{\mathbf{i}} = \text{diag}(\eta_{\mathbf{i},0}, \eta_{\mathbf{i},1}, \dots, \eta_{\mathbf{i},r-1}).$$

164 REMARK 2.2. Here, \hat{U} is a basis matrix that only depends on \mathbf{x}_1 . In fact, if K is replaced
 165 by the interaction between \mathbf{x}_1 and any other separated set, \hat{U} remains the same. Thus, \hat{U} can be
 166 viewed as the *contribution* of \mathbf{x}_1 (to the FMM). \hat{V} can be viewed similarly. An intuitive way of
 167 understanding the matrix form of the FMM is to treat the basis matrices as such contributions
 168 to the FMM.

169 To investigate how the new approximation (2.16) enhances the stability, we give bounds
 170 for the entries of the matrices $\hat{U}, \hat{V}, \hat{B}$. The following lemmas will be used.

171 LEMMA 2.3. *For any integer $r > 0$ and any number $\tau \in (0, \frac{4}{5})$,*

$$(2.19) \quad g_j \equiv \frac{1}{j!} \left(\frac{j}{e} (2\pi r)^{\frac{1}{2r}} \right)^j \leq 1, \quad h_j \equiv \frac{\tau^j}{g_j} < 3\tau, \quad j = 1, 2, \dots, r.$$

172 *Proof.* Let $s = \frac{1}{e} (2\pi r)^{\frac{1}{2r}}$. Then $\frac{1}{e} < s < 1$ and $g_j = \frac{j^j}{j!} s^j$. Since

$$\frac{g_{j+1}}{g_j} = s \left(1 + \frac{1}{j} \right)^j,$$

173 as j increases, g_j either increases monotonically, decreases monotonically, or first decreases
 174 and then increases, depending on r . Thus,

$$g_j \leq \max\{g_1, g_r\} = \max \left\{ s, \frac{(r/e)^r \sqrt{2\pi r}}{r!} \right\} \leq 1.$$

175 To show the second inequality in (2.19), notice that for any $j > 1$,

$$\frac{h_{j+1}}{h_j} = \tau \frac{g_j}{g_{j+1}} = \tau s^{-1} \left(1 + \frac{1}{j} \right)^{-j} < \frac{4}{5} e \left(1 + \frac{1}{j} \right)^{-j} < 1.$$

176 Then for $j > 1$, h_j decreases as j increases. Thus,

$$\max_{j=1, \dots, r} h_j \leq \max\{h_1, h_2\} = \max \left\{ e\tau (2\pi r)^{-\frac{1}{2r}}, \frac{1}{2} (e\tau)^2 (2\pi r)^{-\frac{1}{r}} \right\} < 3\tau.$$

□

177 LEMMA 2.4. *Let k be any positive integer and $\tau > 0$. Then*

$$(2.20) \quad \max_{t \in (0, \tau)} t^j (\tau - t)^{k-j} = \tau^k \left(\frac{j}{k} \right)^j \left(\frac{k-j}{k} \right)^{k-j}, \quad j = 1, 2, \dots, k-1.$$

178 *Proof.* Let $\varphi(t) = t^j (\tau - t)^{k-j}$, $t \in (0, \tau)$. Since

$$\frac{d}{dt} (\log \varphi(t)) = \frac{j}{t} - \frac{k-j}{\tau-t},$$

180 we can see that $\log \varphi(t)$ has only one critical point $t_0 = j\tau/k$ in $(0, \tau)$ for $j < k$. It can
 181 be verified that $\varphi(t_0)$ is the maximum in $(0, \tau)$. Since $\varphi(t_0) = \tau^k \left(\frac{j}{k}\right)^j \left(\frac{k-j}{k}\right)^{k-j}$, we get
 182 (2.20). \square

183 Based on the lemmas, we can estimate the magnitudes of the entries of the matrices
 184 $\hat{U}, \hat{V}, \hat{B}$ in (2.17).

185 **THEOREM 2.5.** *Suppose K is given in (2.10) and \mathbf{x}_1 and \mathbf{x}_2 are two separated sets
 186 with separation ratio $\tau \in (0, \frac{4}{5})$ and with centers z_1 and z_2 , respectively. Then for the
 187 approximation in (2.16)–(2.17), the (i, j) entries of the matrices $\hat{U}, \hat{V}, \hat{B}$ satisfy*

$$|\hat{U}_{ij}| \leq 1, \quad |\hat{V}_{ij}| \leq 1, \quad |\hat{B}_{ij}| \leq \max\{1, 3\tau\} |\kappa(z_1, z_2)|.$$

Proof. According to (2.17), $\hat{U}_{ij} = \eta_{1,j-1} f_{j-1}(x_i - z_1)$, where $\eta_{1,j-1}$ is defined in (2.14). Clearly, $|\hat{U}_{ij}| = 1$ for $j = 1$. For $j = 2, \dots, r$,

(2.21)

$$\begin{aligned} |\hat{U}_{ij}| &= |\eta_{1,j-1} f_{j-1}(x_i - z_1)| = \left(\frac{j-1}{e} (2\pi r)^{\frac{1}{2r}} \frac{1}{\delta_1} \right)^{j-1} \frac{|x_i - z_1|^{j-1}}{(j-1)!} \\ &= \frac{1}{(j-1)!} \left(\frac{j-1}{e} (2\pi r)^{\frac{1}{2r}} \right)^{j-1} \left(\frac{|x_i - z_1|}{\delta_1} \right)^{j-1} = g_{j-1} \cdot \left(\frac{|x_i - z_1|}{\delta_1} \right)^{j-1}, \end{aligned}$$

188 where g_{j-1} is defined following (2.19). By Lemma 2.3, $g_{j-1} \leq 1$. This together with
 189 $|x_i - z_1| \leq \delta_1$ leads to $|\hat{U}_{ij}| \leq 1$. Similarly, $|\hat{V}_{ij}| \leq 1$. We then estimate $|\hat{B}_{ij}|$. According to
 190 (2.9) and (2.17),

$$|\hat{B}_{ij}| = |\alpha_k| \eta_{1,i-1}^{-1} \eta_{2,j-1}^{-1}, \quad i + j \leq r + 1,$$

where $k = i + j - 2$ and α_k is given in (2.6). For $k = 0$ or $i = j = 1$, we simply have
 $|\hat{B}_{11}| = \frac{1}{|z_1 - z_2|}$. For $k \geq 1$, we look at different cases of i, j . For $i = 1$ and $j > 1$, we have
 $\eta_{1,i-1} = 1$ and

$$\begin{aligned} |\hat{B}_{1j}| &= |\alpha_k \eta_{2,j-1}^{-1}| = \frac{(j-1)!}{|z_2 - z_1|^j} \left(\frac{(j-1)}{e} (2\pi r)^{\frac{1}{2r}} \frac{1}{\delta_2} \right)^{-j+1} \\ &= \frac{1}{|z_1 - z_2|} (j-1)! \left(\frac{(j-1)}{e} (2\pi r)^{\frac{1}{2r}} \right)^{-j+1} \left(\frac{\delta_2}{|z_1 - z_2|} \right)^{j-1} \\ &= \frac{1}{|z_1 - z_2|} \frac{1}{g_{j-1}} \left(\frac{\delta_2}{|z_1 - z_2|} \right)^{j-1}. \end{aligned}$$

191 According to (2.3),

$$(2.22) \quad \frac{\delta_2}{|z_1 - z_2|} \leq \frac{\tau \delta_2}{\delta_1 + \delta_2}.$$

192 Then

$$|\hat{B}_{1j}| \leq \frac{1}{|z_1 - z_2|} \frac{\tau^{j-1}}{g_{j-1}} \left(\frac{\delta_2}{\delta_1 + \delta_2} \right)^{j-1} \leq \frac{3\tau}{|z_1 - z_2|} = 3\tau |\kappa(z_1, z_2)|,$$

where Lemma 2.3 is used. For $j = 1$, the derivation is similar to the case when $i = 1$. For $i, j > 1$, we have $2 < k < r$ and

$$\begin{aligned}
 |\hat{B}_{ij}| &= |\alpha_k \eta_{1,i-1}^{-1} \eta_{2,j-1}^{-1}| \\
 &= \frac{k!}{|z_1 - z_2|^{k+1}} \left(\frac{i-1}{e} (2\pi r)^{\frac{1}{2r}} \frac{1}{\delta_1} \right)^{-i+1} \left(\frac{j-1}{e} (2\pi r)^{\frac{1}{2r}} \frac{1}{\delta_2} \right)^{-j+1} \\
 &= \frac{1}{|z_1 - z_2|} k! \left(\frac{1}{e} (2\pi r)^{\frac{1}{2r}} \right)^{-k} (i-1)^{-i+1} (j-1)^{-j+1} \\
 &\quad \cdot \left(\frac{\delta_1}{|z_1 - z_2|} \right)^{i-1} \left(\frac{\delta_2}{|z_1 - z_2|} \right)^{j-1} \\
 &= \frac{1}{|z_1 - z_2|} \frac{k^k}{g_k} (i-1)^{-i+1} (j-1)^{-j+1} \left(\frac{\delta_1}{|z_1 - z_2|} \right)^{i-1} \left(\frac{\delta_2}{|z_1 - z_2|} \right)^{j-1} \\
 &\leq \frac{1}{|z_1 - z_2|} \frac{k^k}{g_k} (i-1)^{-i+1} (j-1)^{-j+1} \left(\frac{\tau \delta_1}{\delta_1 + \delta_2} \right)^{i-1} \left(\frac{\tau \delta_2}{\delta_1 + \delta_2} \right)^{j-1},
 \end{aligned}$$

where $\frac{\delta_1}{|z_1 - z_2|} \leq \frac{\tau \delta_1}{\delta_1 + \delta_2}$ and (2.22) are used. By setting $t = \frac{\tau \delta_1}{\delta_1 + \delta_2} < \tau$ in Lemma 2.4, we further get

$$\begin{aligned}
 |\hat{B}_{ij}| &\leq \frac{1}{|z_1 - z_2|} \frac{k^k}{g_k} (i-1)^{-i+1} (j-1)^{-j+1} \tau^k \left(\frac{i-1}{k} \right)^{i-1} \left(\frac{j-1}{k} \right)^{j-1} \\
 &= \frac{1}{|z_1 - z_2|} \frac{\tau^k}{g_k} \leq \frac{3\tau}{|z_1 - z_2|} = 3\tau |\kappa(z_1, z_2)|,
 \end{aligned}$$

193 where Lemma 2.3 is used. This completes the proof. □

194 Hence, the entries of the basis matrices \hat{U} and \hat{V} in (2.17) have magnitudes bounded
 195 by 1. \hat{B} is just a small matrix with order r and its entries have magnitudes bounded by a
 196 small multiple of $|\kappa(z_1, z_2)|$ which depends on the two centers only. These bounds ensure the
 197 stability of matrix operations with the low-rank approximation $\hat{U} \hat{B} \hat{V}^T$. See Section 2.5 later.

198 REMARK 2.6. It is clear that our scaling strategy can control the entrywise magnitudes
 199 of not only \hat{U}, \hat{V} , but also \hat{B} . This is a significant advantage over simple methods such
 200 as straightforward scaling/normalization of the columns of \hat{U}, \hat{V} . The latter can make the
 201 entries of the resulting \hat{B} matrix poorly scaled or even cause numerical overflow. Even if the
 202 simple scaling factors from the latter strategy can be represented as separate diagonal matrices,
 203 forming these scaling factors and the entries of \hat{B} in a separate manner can pose numerical
 204 issues (since they may still be very large for some cases). The entries of \hat{B} may still be much
 205 larger than the original entries in K and thus not be well controlled. With our strategy, the
 206 entrywise magnitudes of \hat{B} are under control and we can integrate our scaling factors into the
 207 computation of the entries of \hat{B} if needed.

208 **2.3. Stable translation relation and analysis of entrywise magnitudes.** A key idea for
 209 the FMM to reach linear complexity is to exploit a *translation relation* between the so-called
 210 local expansions associated with one point set and its subsets [16]. This is essentially to use
 211 nested basis matrices in off-diagonal approximations. Here, we give an explicit matrix relation
 212 that ensures stable operations. To facilitate later discussions, we assume a set $\mathbf{x}_i \subset \mathbf{s}$ has
 213 center z_i and radius δ_i , as mentioned at the beginning of Section 2.2, and a subset $\mathbf{x}_c \subset \mathbf{x}_i$ has
 214 center z_c and radius δ_c .

As mentioned in Remark 2.2, we can derive a basis matrix \hat{U}_i as the contribution of \mathbf{x}_i and a basis matrix \hat{U}_c as the contribution of \mathbf{x}_c . In the FMM, the translation relation is used to

connect \hat{U}_c to the contribution of \mathbf{x}_c to \hat{U}_i . Specifically, the translation relation in our context can be derived for f_j in (2.6) as follows:

$$(2.23) \quad \begin{aligned} f_j(x - z_i) &= \frac{(x - z_i)^j}{j!} = \frac{((x - z_c) + (z_c - z_i))^j}{j!} \\ &= \sum_{i=0}^j \frac{(x - z_c)^i}{i!} \frac{(z_c - z_i)^{j-i}}{(j-i)!} = \sum_{l=0}^j (\eta_{c,i} f_l(x - z_c)) (\eta_{c,i}^{-1} f_{j-i}(z_c - z_i)), \end{aligned}$$

where we have included the scaling factor $\eta_{c,i}$ for stability purpose. Therefore, a row in \hat{U}_i can be written as

$$(2.24) \quad \begin{aligned} &[\eta_{i,0} f_0(x - z_i) \quad \dots \quad \eta_{i,r-1} f_{r-1}(x - z_i)] \\ &= [\eta_{c,0} f_0(x - z_c) \quad \dots \quad \eta_{c,r-1} f_{r-1}(x - z_c)] T_{c,i}, \end{aligned}$$

215 where $[\eta_{c,0} f_0(x - z_c) \quad \dots \quad \eta_{c,r-1} f_{r-1}(x - z_c)]$ is a row of \hat{U}_c and $T_{c,i}$ is the *translation*
216 *matrix*

$$(2.25) \quad T_{c,i} = S_c^{-1} \begin{bmatrix} f_0(z_c - z_i) & \dots & f_{r-1}(z_c - z_i) \\ & \ddots & \vdots \\ & & f_0(z_c - z_i) \end{bmatrix} S_i,$$

217 with S_i in (2.18) and S_c defined in the same way. With the translation matrix $T_{c,i}$, the
218 contribution of x to \hat{U}_c is related to the contribution of x to \hat{U}_i as in (2.24).

219 We then study the entrywise magnitudes of $T_{c,i}$. To accommodate the general situation
220 that \mathbf{x}_c may be any subset of \mathbf{x}_i resulting from the partitioning of \mathbf{x}_i , we suppose

$$(2.26) \quad \delta_i - \delta_c \geq |z_c - z_i|,$$

221 so that the disk defined by $|x - z_c| \leq \delta_c$ (that encloses \mathbf{x}_c) is fully located inside the disk
222 $|x - z_i| \leq \delta_i$ (that encloses \mathbf{x}_i).

223 **THEOREM 2.7.** *Suppose (2.26) holds. Then the (i, j) entry $(T_{c,i})_{i,j}$ of $T_{c,i}$ defined in
224 (2.25) satisfies $|(T_{c,i})_{i,j}| \leq 1$.*

225 *Proof.* $T_{c,i}$ is an upper triangular matrix and the (i, j) entry for $1 \leq i \leq j \leq r$ is

$$(T_{c,i})_{i,j} = \eta_{i,j-1} \eta_{c,i-1}^{-1} f_{j-i}(z_c - z_i).$$

226 If $j = 1$, $(T_{c,i})_{i,j} = 1$. Then suppose $j > 1$. We look at different cases of i .

1. When $i = 1$, just like the derivation in (2.21),

$$\begin{aligned} |(T_{c,i})_{i,j}| &= |\eta_{i,j-1} f_{j-1}(z_c - z_i)| = \left(\frac{j-1}{e} (2\pi r)^{\frac{1}{2r}} \frac{1}{\delta_i} \right)^{j-1} \frac{|z_c - z_i|^{j-1}}{(j-1)!} \\ &= g_{j-1} \cdot \left(\frac{|z_c - z_i|}{\delta_i} \right)^{j-1} \leq 1, \end{aligned}$$

227 where Lemma 2.3 and (2.26) are used.

2. When $1 < i < j$,

$$\begin{aligned}
 |(T_{\mathbf{c},\mathbf{i}})_{i,j}| &= (j-1)^{j-1}(i-1)^{-i+1} \left(\frac{1}{e} (2\pi r)^{\frac{1}{2r}} \right)^{j-i} \frac{\delta_{\mathbf{c}}^{i-1} |z_{\mathbf{c}} - z_{\mathbf{i}}|^{j-i}}{\delta_{\mathbf{i}}^{j-1} (j-i)!} \\
 &\leq (j-1)^{j-1}(i-1)^{-i+1} \frac{1}{(j-i)!} \left(\frac{1}{e} (2\pi r)^{\frac{1}{2r}} \right)^{j-i} \left(\frac{\delta_{\mathbf{c}}}{\delta_{\mathbf{i}}} \right)^{i-1} \left(1 - \frac{\delta_{\mathbf{c}}}{\delta_{\mathbf{i}}} \right)^{j-i} \\
 &\quad (\text{by (2.26)}) \\
 &\leq (j-1)^{j-1}(i-1)^{-i+1} \frac{1}{(j-i)!} \left(\frac{1}{e} (2\pi r)^{\frac{1}{2r}} \right)^{j-i} \left(\frac{i-1}{j-1} \right)^{i-1} \left(\frac{j-i}{j-1} \right)^{j-i} \\
 &\quad (\text{by Lemma 2.4}) \\
 &= \frac{1}{(j-i)!} \left(\frac{j-i}{e} (2\pi r)^{\frac{1}{2r}} \right)^{j-i} = g_{j-i} \leq 1,
 \end{aligned}$$

228 where the last inequality is due to Lemma 2.3.

229 3. When $i = j$,

$$|(T_{\mathbf{c},\mathbf{i}})_{i,j}| = |\eta_{\mathbf{i},i-1} \eta_{\mathbf{c},i-1}^{-1}| = \left(\frac{\delta_{\mathbf{c}}}{\delta_{\mathbf{i}}} \right)^{i-1} \leq 1.$$

230 \square

231 In Section 3.1, we show how the translation matrix $T_{\mathbf{c},\mathbf{i}}$ is used to build a nested basis
 232 form for $\hat{U}_{\mathbf{i}}$.

233 REMARK 2.8. It is worth pointing out that there are also other analytical methods that can
 234 produce translation matrices that satisfy similar entrywise bounds. For example, the method
 235 in [15] uses an integral form and quadrature approximation to obtain translation operators in
 236 diagonal forms with entrywise magnitudes bounded by 1. On the other hand, the resulting
 237 basis matrices depend on the quadrature weights and bounds on their entries are not studied in
 238 [15]. Here, our idea is to integrate scaling into simple Taylor expansions so as to control the
 239 entrywise magnitudes of all the relevant matrices.

240 **2.4. Generalizations.** It can be shown that our results can be generalized to various
 241 useful kernels like $1/(x-y)^k$ with integer $k > 0$, $\log(x-y)$, $\log|x-y|$, and other kernels
 242 with expansions similar to (2.5). In fact, by using the same set of scaling factors as in Section
 243 2.2, we can get bounds similar to those in Theorem 2.5. That is, the entrywise bound for the
 244 \hat{U}, \hat{V} basis matrices remain to be 1. The relative entrywise bound for the \hat{B} generators only
 245 changes slightly. In our numerical tests in Section 4, tests for different kernels will be given.
 246 For some kernels that do not have similar Taylor expansions, the stabilization is beyond the
 247 scope of this work.

248 **2.5. Stability.** Our stabilization strategies ensure the stability of operations involving the
 249 resulting structured forms in the FMM. For example, the stability of multiplying $\hat{U}\hat{B}\hat{V}^T$ and
 250 vectors can be shown as follows.

251 THEOREM 2.9. *For the $m \times p$ interaction matrix K in (2.10), suppose the same conditions
 252 as in Theorem 2.5 hold and $\hat{K} = \hat{U}\hat{B}\hat{V}^T$ is the approximation to K as in (2.16)–(2.17). Then
 253 the matrix-vector multiplication $\hat{b} = \hat{U}\hat{B}\hat{V}^T w \approx Kw$ for a vector w satisfies*

$$\begin{aligned}
 \text{fl}(\hat{b}) &= (\hat{U}\hat{B}\hat{V}^T + \Delta\hat{K})w, \quad \text{with} \\
 \|\Delta\hat{K}\|_F &\leq \max\{1, 3\tau\}(1+\tau)r^2\sqrt{mp}\gamma_{p+2r}\|K\|_F + \mathcal{O}(\epsilon_{\text{mach}}^2),
 \end{aligned}$$

251 where $\text{fl}(\cdot)$ denotes the numerical result in floating point operations, ϵ_{mach} denotes the machine
 252 epsilon, and $\gamma_k = \frac{k\epsilon_{\text{mach}}}{1-k\epsilon_{\text{mach}}}$.

253 *Proof.* It is commonly known that (see, e.g., [22]), for a matrix C with column size p , the
 254 matrix-vector multiplication Cw satisfies the following backward error result:

$$\text{fl}(Cw) = (C + \Delta C)w, \quad |\Delta C| \leq \gamma_p |C|.$$

Thus, when the matrix-vector multiplication $\hat{K}w = \hat{U}\hat{B}\hat{V}^T w$ is considered, we have

$$\begin{aligned} b_1 &= \text{fl}(\hat{V}^T w) = (\hat{V}^T + \Delta \hat{V}^T)w, \quad |\Delta \hat{V}^T| \leq \gamma_p |\hat{V}^T|, \\ b_2 &= \text{fl}(\hat{B}b_1) = (\hat{B} + \Delta \hat{B})b_1, \quad |\Delta \hat{B}| \leq \gamma_r |\hat{B}|, \\ \hat{b} &= \text{fl}(\hat{U}b_2) = (\hat{U} + \Delta \hat{U})b_2, \quad |\Delta \hat{U}| \leq \gamma_r |\hat{U}|. \end{aligned}$$

255 (Note that \hat{K} is $m \times p$ and \hat{B} is $r \times r$.) Combining these results, we get

$$\text{fl}(\hat{U}\hat{B}\hat{V}^T w) = (\hat{U} + \Delta \hat{U})(\hat{B} + \Delta \hat{B})(\hat{V}^T + \Delta \hat{V}^T)w \equiv (\hat{U}\hat{B}\hat{V}^T + \Delta \hat{K})w,$$

where

$$\begin{aligned} \|\Delta \hat{K}\|_F &\leq \|\hat{U}\hat{B}(\Delta \hat{V}^T)\|_F + \|\hat{U}(\Delta \hat{B})\hat{V}^T\|_F + \|(\Delta \hat{U})\hat{B}\hat{V}^T\|_F + \mathcal{O}(\epsilon_{\text{mach}}^2) \\ &\leq (\gamma_p + 2\gamma_r) \|\hat{U}\|_F \|\hat{B}\|_F \|\hat{V}\|_F + \mathcal{O}(\epsilon_{\text{mach}}^2). \end{aligned}$$

(Here, we use Frobenius norm in the backward error instead of the max-norm since the former is sub-multiplicative but the latter is not.) According to Theorem 2.5, we have

$$\begin{aligned} \|\hat{U}\|_F &\leq \sqrt{mr} \|\hat{U}\|_{\max} \leq \sqrt{mr}, \quad \|\hat{V}\|_F \leq \sqrt{rq} \|\hat{V}\|_{\max} \leq \sqrt{rq}, \\ \|\hat{B}\|_F &\leq r \|\hat{B}\|_{\max} \leq r \max\{1, 3\tau\} |\kappa(z_1, z_2)|, \end{aligned}$$

where z_1 and z_2 are the centers of \mathbf{x}_1 and \mathbf{x}_2 in (2.10), respectively. Due to the separation condition in Definition 2.1, we have (2.7) for any $x \in \mathbf{x}_1$ and $y \in \mathbf{x}_2$. Thus,

$$\|\hat{B}\|_F \leq r \max\{1, 3\tau\} (1 + \tau) |\kappa(x, y)| \leq r \max\{1, 3\tau\} (1 + \tau) \|K\|_F.$$

Accordingly,

$$\begin{aligned} \|\Delta \hat{K}\|_F &\leq (\gamma_p + 2\gamma_r) \sqrt{mr} \sqrt{rp} (r \max\{1, 3\tau\} (1 + \tau) \|K\|_F) + \mathcal{O}(\epsilon_{\text{mach}}^2) \\ &= \max\{1, 3\tau\} (1 + \tau) r^2 \sqrt{mp} \frac{(p + 2r) \epsilon_{\text{mach}} - 3rp \epsilon_{\text{mach}}^2}{1 - (p + r) \epsilon_{\text{mach}} + rp \epsilon_{\text{mach}}^2} \|K\|_F + \mathcal{O}(\epsilon_{\text{mach}}^2) \\ &\leq \max\{1, 3\tau\} (1 + \tau) r^2 \sqrt{mp} \gamma_{p+2r} \|K\|_F + \mathcal{O}(\epsilon_{\text{mach}}^2). \end{aligned}$$

256

257 This theorem shows the backward stability of using the low-rank approximation \hat{K} to
 258 compute the matrix-vector product $\hat{K}w$ that approximates Kw . (For this reason, it makes
 259 somewhat more sense to use K in the backward error bound.) □

260 Note that, if no scaling is used like in the usual FMM, then $\|\hat{U}\|_{\max}$, $\|\hat{V}\|_{\max}$, and/or
 261 $\|\hat{B}\|_{\max}$ may potentially get very large, leading to significantly larger backward error bounds.
 262 The impact can be observed from the numerical results later.

263 **3. Extension of the stabilization from FMM to HSS matrices.** We then show an
 264 example of an intuitive analytical construction of an FMM matrix satisfying some stability
 265 requirements and, moreover, extend the stabilization from the FMM matrix to an HSS form.
 266 This further connects the FMM with stable and fast ULV factorizations for HSS matrices.

267 **3.1. An example for the FMM matrix representation.** We first integrate the stabilization
 268 strategy in the previous section into the FMM framework for constructing an FMM matrix
 269 example. For convenience, we consider the 1D case and suppose the set of points s in (1.1) is
 270 located in an interval $\mathcal{I} \subset \mathbb{R}$. Note that 1D cases are very useful for many different situations
 271 [5, 8, 13, 25, 26, 31, 33]. (The 1D point set is also just used to simplify the presentation. The
 272 strategy below can be easily adapted to more general 1D curves. The essential ideas can also
 273 be extended to 2D sets.) We consider A in (1.2) as the discretization of κ in (2.2) on s . Given
 274 an accuracy ε , we follow a general framework in [32] and use the 1D FMM scheme to produce
 275 an FMM matrix \hat{A} such that

$$(3.1) \quad A = \hat{A} + A \odot E, \quad \text{with } |E_{ij}| \leq \varepsilon.$$

276 According to (2.13), r can be chosen to make $\tau^r \frac{1+\tau}{1-\tau} \leq \varepsilon$.

277 **3.1.1. Set partitioning and far-field interaction.** To conveniently organize the FMM
 278 matrix representation, we use a postordered binary tree \mathcal{T} with nodes $i = 1, 2, \dots, \text{root}(\mathcal{T})$,
 279 where $\text{root}(\mathcal{T})$ denotes the root node. See Figure 3.1. Suppose \mathcal{T} has L levels such that
 280 $n/2^{L-1} = \mathcal{O}(r)$ and $\text{root}(\mathcal{T})$ is at level 0. Partition the set s hierarchically following \mathcal{T} .
 281 That is, suppose each node i is associated with a subset $x_i \subset s$ so that $x_{\text{root}(\mathcal{T})} = s$ and
 282 $x_i = x_{c_1} \cup x_{c_2}, x_{c_1} \cap x_{c_2} = \emptyset$ for any nonleaf node i with children c_1 and c_2 . Based on the
 283 subinterval where x_i is located, we can conveniently determine a center z_i and a radius δ_i of
 284 x_i . For each leaf i , the cardinality $m_i \equiv |x_i| = \mathcal{O}(r)$.

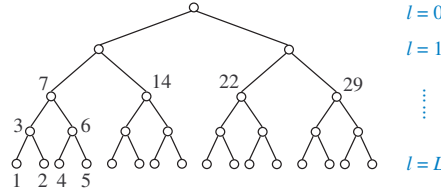


FIG. 3.1. Example of a postordered tree \mathcal{T} used for the FMM.

284 Later for convenience, when x_i is used, we may simply refer to node i of \mathcal{T} . For example,
 285 given two nodes i and j of \mathcal{T} corresponding to two separated sets x_i and x_j (as defined in
 286 Definition 2.1), respectively, we just say i and j are separated.

287 Suppose x_i corresponds to the index set \mathcal{I}_i so that the submatrix of A corresponding to
 288 the row index set \mathcal{I}_i and column index set \mathcal{I}_j is $A|_{\mathcal{I}_i \times \mathcal{I}_j} = (\kappa(x_i, x_j))_{x_i \in x_i, x_j \in x_j}$, which is
 289 the interaction between i and j . When i and j are separated, $A|_{\mathcal{I}_i \times \mathcal{I}_j}$ can be approximated by a
 290 low-rank form like in (2.16) and is said to be a *far-field* interaction. For notational convenience,
 291 we rewrite (2.16) as

$$(3.2) \quad A|_{\mathcal{I}_i \times \mathcal{I}_j} = \hat{U}_i \hat{B}_{i,j} \hat{V}_j^T + A|_{\mathcal{I}_i \times \mathcal{I}_j} \odot E_{i,j} \approx \hat{U}_i \hat{B}_{i,j} \hat{V}_j^T,$$

293 where appropriate sets used for the definition of the matrices in (2.17) are replaced by x_i and
 294 x_j . Correspondingly, the centers z_i, z_j , the radii δ_i, δ_j , and the scaling factors $\eta_{i,j}, \eta_{j,j}$ as in
 295 (2.14) are used for the definition of $\hat{U}_i, \hat{B}_{i,j}, \hat{V}_j^T$ in (3.2).

296 As mentioned in Remark 2.2, we call \hat{U}_i the *contribution* (matrix) from node i . Clearly,
 297 $\hat{U}_i = \hat{V}_i$. However, to accommodate more general matrix forms, we still use \hat{V}_i^T for the row
 298 basis matrix in (3.2).

299 When \mathbf{i} and \mathbf{j} are not separated, they are said to be *near neighbors*, and $A|_{\mathcal{I}_i \times \mathcal{I}_j}$ is a
 300 *near-field* interaction. Near-field interactions may be further partitioned so as to generate
 301 far-field interactions at finer levels.

302 **3.1.2. Levelwise low-rank approximation.** In the FMM, far-field interactions are orga-
 303 nized with the aid of *interaction lists* [16], which encode the interactions to consider at each
 304 level of partition. Specifically for our case, the *interaction list* \mathcal{L}_i for node \mathbf{i} of \mathcal{T} is the set of
 305 nodes \mathbf{j} at the same level as \mathbf{i} but well-separated from \mathbf{i} , and with its parent a near neighbor of
 306 \mathbf{i} .

307 Corresponding to level l of \mathcal{T} , let $A^{(l)}$ be the submatrix extracted from A by retaining
 308 only the blocks $A|_{\mathcal{I}_i \times \mathcal{I}_j}$ for all nodes \mathbf{i} at level l and $\mathbf{j} \in \mathcal{L}_i$ and zeroing out other blocks
 309 in A . For example, for $l = 2$, the four nodes in Figure 3.1 have interaction lists $\mathcal{L}_7 =$
 310 $\{22, 29\}$, $\mathcal{L}_{14} = \{29\}$, $\mathcal{L}_{22} = \{7\}$, $\mathcal{L}_{29} = \{7, 14\}$. The corresponding far-field interactions
 311 are shown in Figure 3.2(a). Similarly, the far-field interactions for $l = 3, 4$ are shown in Figure
 312 3.2(b–c). Correspondingly, the matrix A can be decomposed levelwise into the following sum
 313 of matrices corresponding to far-field interactions and near-field interactions:

$$(3.3) \quad A = A^{(2)} + \cdots + A^{(L)} + A^{(N)},$$

314 where $A^{(N)}$ denotes all the near-field interactions at the leaf level L of the partition. $A^{(N)}$ is a
 315 block banded matrix.

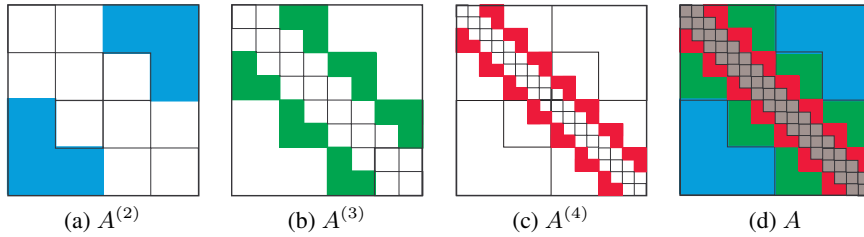


FIG. 3.2. Nonzero patterns of $A^{(l)}$ and how $A^{(l)}$ appears in A , where the grey band in (d) corresponds to $A^{(N)}$.

For $l \geq 2$, the nonzero block $A|_{\mathcal{I}_i \times \mathcal{I}_j}$ for each node \mathbf{i} at level l and $\mathbf{j} \in \mathcal{L}_i$ has a low-rank
 approximation as in (3.2). For convenience, let $\mathbf{i}_1, \dots, \mathbf{i}_\beta$ be the nodes at level l of \mathcal{T} , ordered
 from left to right. Then, we can write

$$(3.4) \quad A^{(l)} = \hat{U}^{(l)} \hat{B}^{(l)} (\hat{V}^{(l)})^T + A^{(l)} \odot E^{(l)} \approx \hat{U}^{(l)} \hat{B}^{(l)} (\hat{V}^{(l)})^T, \quad \text{with}$$

$$(3.5) \quad \hat{U}^{(l)} = \text{diag}(\hat{U}_{\mathbf{i}_1}, \dots, \hat{U}_{\mathbf{i}_\beta}), \quad \hat{V}^{(l)} = \text{diag}(\hat{V}_{\mathbf{i}_1}, \dots, \hat{V}_{\mathbf{i}_\beta}),$$

316 and $\hat{B}^{(l)}$ and $E^{(l)}$ have the same block nonzero patterns as $A^{(l)}$ with the nonzero blocks
 317 $A|_{\mathcal{I}_i \times \mathcal{I}_j}$ of $A^{(l)}$ replaced by $\hat{B}_{i,j}$ and $E_{i,j}$, respectively. See Figure 3.3.

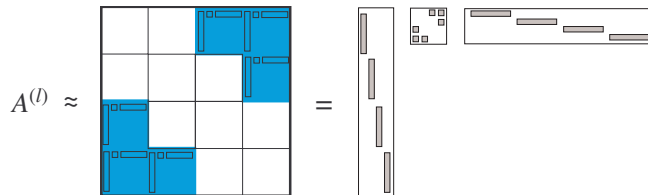


FIG. 3.3. Nonzero patterns of $\hat{U}^{(l)}$, $\hat{B}^{(l)}$, and $\hat{V}^{(l)}$ in (3.4) for $A^{(l)}$ with $l = 2$ in Figure 3.2(a).

318 From (3.3) and (3.4), we have the following approximation of A :

$$(3.6) \quad A = \sum_{l=2}^L \hat{U}^{(l)} \hat{B}^{(l)} (\hat{V}^{(l)})^T + A^{(N)} + A \odot E \approx \sum_{l=2}^L \hat{U}^{(l)} \hat{B}^{(l)} (\hat{V}^{(l)})^T + A^{(N)} \equiv \hat{A},$$

319 where $E = E^{(2)} + \dots + E^{(L)}$. Since the nonzero blocks of $E^{(l)}$ for different l do not overlap,
 320 E satisfies the bound in (3.1).

321 Thus, \hat{A} is an approximation to A with entrywise relative accuracy ε as in (3.1). It can be
 322 easily seen that \hat{A} can be used to compute matrix-vector products in $\mathcal{O}(rnL) = \mathcal{O}(rn \log n)$
 323 flops with $r = \mathcal{O}(|\log \varepsilon|)$. Assume ε is fixed and then this cost becomes $\mathcal{O}(n \log n)$.

3.1.3. Nested basis and FMM matrix in a telescoping expansion form. The essential strategy to reduce the matrix-vector multiplication cost from $\mathcal{O}(n \log n)$ to $\mathcal{O}(n)$ in the FMM is to use nested basis matrices in the off-diagonal approximations. This can utilize the translation relation in Section 2.3. According to the relation in (2.24), the basis matrices or contributions from a parent node \mathbf{i} of \mathcal{T} and its children \mathbf{c}_1 and \mathbf{c}_2 are related by

$$(3.7) \quad \hat{U}_{\mathbf{i}} = \begin{bmatrix} \hat{U}_{\mathbf{c}_1} & \\ & \hat{U}_{\mathbf{c}_2} \end{bmatrix} \begin{bmatrix} \hat{R}_{\mathbf{c}_1} \\ \hat{R}_{\mathbf{c}_2} \end{bmatrix}, \quad \hat{V}_{\mathbf{i}} = \begin{bmatrix} \hat{V}_{\mathbf{c}_1} & \\ & \hat{V}_{\mathbf{c}_2} \end{bmatrix} \begin{bmatrix} \hat{W}_{\mathbf{c}_1} \\ \hat{W}_{\mathbf{c}_2} \end{bmatrix}, \quad \text{with}$$

$$(3.8) \quad \hat{R}_{\mathbf{c}_1} = \hat{W}_{\mathbf{c}_1} = T_{\mathbf{c}_1, \mathbf{i}}, \quad \hat{R}_{\mathbf{c}_2} = \hat{W}_{\mathbf{c}_2} = T_{\mathbf{c}_2, \mathbf{i}}.$$

324 (3.7) shows how the nested basis matrices are obtained.

325 REMARK 3.1. Note that the translation relation (2.23) is a result of the binomial expansion.
 326 Although here \mathbf{c}_1 and \mathbf{c}_2 are children of \mathbf{i} , the translation relation in Section 2.3 is not restricted
 327 to the case where \mathbf{c} is a child of \mathbf{i} . That is, $T_{\mathbf{c}, \mathbf{i}}$ in (2.25) can be used for any descendant \mathbf{c} of \mathbf{i} .

The approximation in (3.6) can then be converted into a nested form. That is, let

$$(3.9) \quad \begin{aligned} \hat{U}^{(l)} &= \hat{U}^{(l+1)} \hat{R}^{(l+1)}, \quad \hat{V}^{(l)} = \hat{V}^{(l+1)} \hat{W}^{(l+1)}, \quad l = 1, 2, \dots, L-1, \quad \text{with} \\ \hat{R}^{(l+1)} &= \text{diag} \left(\begin{bmatrix} \hat{R}_{\mathbf{c}_1} \\ \hat{R}_{\mathbf{c}_2} \end{bmatrix}, \mathbf{c}_1, \mathbf{c}_2: \text{children of each node } \mathbf{i} \text{ at level } l \right), \\ \hat{W}^{(l+1)} &= \text{diag} \left(\begin{bmatrix} \hat{W}_{\mathbf{c}_1} \\ \hat{W}_{\mathbf{c}_2} \end{bmatrix}, \mathbf{c}_1, \mathbf{c}_2: \text{children of each node } \mathbf{i} \text{ at level } l \right). \end{aligned}$$

328 We can then rewrite the approximation in (3.4) as a recursive relation

$$(3.10) \quad \hat{U}^{(l)} \hat{B}^{(l)} (\hat{V}^{(l)})^T = \hat{U}^{(L)} \hat{R}^{(L-1)} \dots \hat{R}^{(l)} \hat{B}^{(l)} (\hat{W}^{(l)})^T \dots (\hat{W}^{(L-1)})^T (\hat{V}^{(L)})^T,$$

329 where $\hat{U}^{(L)}$ and $\hat{V}^{(L)}$ are defined for the leaf level L as in (3.5).

Inserting (3.10) into (3.6), we obtain the following *telescoping expansion* of \hat{A} :

$$(3.11) \quad \begin{aligned} \hat{A} &= \hat{U}^{(L)} \left(\hat{R}^{(L-1)} \left(\dots \left(\hat{R}^{(2)} \hat{B}^{(2)} (\hat{W}^{(2)})^T + \hat{B}^{(3)} \right) \dots \right) (\hat{W}^{(L-1)})^T + \hat{B}^{(L)} \right) (\hat{V}^{(L)})^T + A^{(N)}, \end{aligned}$$

330 which is the hierarchical matrix form produced by the FMM or the *FMM matrix*. For convenience,
 331 we call the matrices $\hat{U}_{\mathbf{i}}, \hat{V}_{\mathbf{i}}, \hat{R}_{\mathbf{i}}, \hat{W}_{\mathbf{i}}, \hat{B}_{\mathbf{i}}$ *FMM generators*. We also suppose that each
 332 node \mathbf{i} of the FMM tree \mathcal{T} is associated with FMM generators $\hat{U}_{\mathbf{i}}, \hat{V}_{\mathbf{i}}, \hat{R}_{\mathbf{i}}, \hat{W}_{\mathbf{i}}, \hat{B}_{\mathbf{i}}$. Due to the
 333 nested bases, the $\hat{U}_{\mathbf{i}}, \hat{V}_{\mathbf{i}}$ generators associated with a nonleaf node \mathbf{i} are not explicitly stored.
 334 The total storage for the FMM matrix \hat{A} is then just $\mathcal{O}(rn)$. The cost to multiply the FMM
 335 matrix and a vector now becomes $\mathcal{O}(rn)$.

336 **3.2. General idea of transforming FMM into HSS matrices.** We now consider the
 337 conversion of the FMM matrix \hat{A} in (3.11) into an HSS form. Note that in [3, 38, 39], the
 338 construction of HSS matrices is based on algebraic strategies. It is also possible to use
 339 analytical compression like the methods in [25, 41, 42, 43] for HSS constructions, but it is
 340 unclear whether the resulting HSS forms satisfy the stability requirements or not. Here, we
 341 use an analytical way to convert the FMM matrix to an HSS form. The resulting HSS form
 342 has a generator representation with the generators satisfying proper norm bounds.

An HSS matrix can be organized with the aid of a binary tree called HSS tree [38]. Here, we can use the same binary tree \mathcal{T} like in Figure 3.1. An HSS form for \hat{A} can be defined with the aid of a set of *HSS generators* $D_i, U_i, V_i, R_i, W_i, B_i$:

$$(3.12) \quad \hat{A} = D_{\text{root}(\mathcal{T})}, \quad D_i = \begin{bmatrix} D_{c_1} & U_{c_1} B_{c_1} V_{c_2}^T \\ U_{c_2} B_{c_2} V_{c_1}^T & D_{c_2} \end{bmatrix},$$

$$(3.13) \quad U_i = \begin{bmatrix} U_{c_1} \\ U_{c_2} \end{bmatrix} \begin{bmatrix} R_{c_1} \\ R_{c_2} \end{bmatrix}, \quad V_i = \begin{bmatrix} V_{c_1} \\ V_{c_2} \end{bmatrix} \begin{bmatrix} W_{c_1} \\ W_{c_2} \end{bmatrix},$$

343 where c_1, c_2 are the left and right children of a nonleaf node i , respectively.

344 Use $\{1 : n\}$ to denote the set $\{1, 2, \dots, n\}$. Also, let \mathcal{I}_i be the index set associated with
 345 D_i such that $D_i = \hat{A}|_{\mathcal{I}_i \times \mathcal{I}_i}$. Then we see from (3.12)–(3.13) that the columns of U_i span the
 346 column space of the block $A|_{\mathcal{I}_i \times (\{1:n\} \setminus \mathcal{I}_i)}$. Similarly, the columns of V_i span the column space
 347 of the block $(A|_{(\{1:n\} \setminus \mathcal{I}_i) \times \mathcal{I}_i})^T$. (3.13) indicates that the U_i, V_i basis matrices have nested
 348 forms.

The HSS form also has a telescoping expansion [24]:

$$(3.14) \quad \hat{A} = U^{(L)} \left(R^{(L-1)} \left(\dots \left(R^{(2)} B^{(1)} (W^{(2)})^T + B^{(2)} \right) \dots \right) (W^{(L-1)})^T + B^{(L-1)} \right) \\ \cdot (V^{(L)})^T + D^{(L)},$$

349 where

$$D^{(L)} = \text{diag}(D_i, i: \text{each node at level } L),$$

$$U^{(L)} = \text{diag}(U_i, i: \text{each node at level } L),$$

$$V^{(L)} = \text{diag}(V_i, i: \text{each node at level } L),$$

$$R^{(l)} = \text{diag} \left(\begin{bmatrix} R_{c_1} \\ R_{c_2} \end{bmatrix}, c_1, c_2: \text{children of each node } i \text{ at level } l < L \right),$$

$$W^{(l)} = \text{diag} \left(\begin{bmatrix} W_{c_1} \\ W_{c_2} \end{bmatrix}, c_1, c_2: \text{children of each node } i \text{ at level } l < L \right),$$

$$B^{(l)} = \text{diag} \left(\begin{bmatrix} 0 & B_{c_1} \\ B_{c_2} & 0 \end{bmatrix}, c_1, c_2: \text{children of each node } i \text{ at level } l < L \right).$$

350 The telescoping expansion in (3.14) has a form similar to the expansion in (3.11) for the FMM.
 351 These two telescoping expansions have the following differences:

- 352 • In (3.11), the last term $A^{(N)}$ for the near-field interactions has a block banded form,
 353 while in (3.14), only the diagonal blocks are considered as near-field interactions so
 354 that the last term $D^{(L)}$ has a block diagonal form.
- 355 • Accordingly, the $\hat{U}^{(L)}, \hat{V}^{(L)}$ basis matrices in (3.11) are different from $U^{(L)}, V^{(L)}$
 356 in (3.14), respectively, since they are basis matrices for different off-diagonal blocks.
 357 $\hat{R}^{(l)}, \hat{W}^{(l)}$ in (3.11) are also different from $R^{(l)}, W^{(l)}$ in (3.14), respectively.
- 358 • In (3.11), $\hat{B}^{(l)}$ has a block nonzero pattern similar to $A^{(l)}$ illustrated in Figure 3.2,
 359 while in (3.14), $B^{(l)}$ has a block-diagonal form.

360 We will resolve these differences by showing how to construct an HSS form from the
 361 FMM form. It should be noted that the HSS form we are constructing is for the FMM matrix
 362 \hat{A} in (3.11). That is, we are constructing an HSS approximation to A .

363 The basic idea of constructing the HSS form of \hat{A} is to find HSS representations for the
 364 *far-field matrix* $\hat{A}^{(F)} \equiv \hat{A} - A^{(N)}$ and the near-field matrix $A^{(N)}$ separately and then to merge
 365 the two sets of HSS generators. In Figure 3.2(d), $A^{(N)}$ corresponds to the grey banded matrix
 366 along the diagonal and $\hat{A}^{(F)}$ corresponds to the remaining part of the matrix. To distinguish
 367 the generators for different matrices, we use the following notation.

- 368 • \hat{U}, \hat{V} , etc.: FMM generators of $\hat{A}^{(F)}$ from the FMM procedure in Section 3.1.
- 369 • U, V , etc.: HSS generators for the HSS form of \hat{A} .
- 370 • \tilde{U}, \tilde{V} , etc.: HSS generators for the HSS form of $\hat{A}^{(F)}$.
- 371 • \check{U}, \check{V} , etc.: HSS generators for the HSS form of $A^{(N)}$.

372 The HSS representation for the near-field part $A^{(N)}$ can be explicitly written out based on
 373 its block banded form. The main task is then to find the HSS representation of the far-field
 374 part $\hat{A}^{(F)}$. We do this in two steps:

375 1. First, we write each off-diagonal block in a low-rank form

$$(3.15) \quad \hat{A}^{(F)}|_{\mathcal{I}_i \times \mathcal{I}_j} = \tilde{U}_i \tilde{B}_i \tilde{V}_j^T,$$

376 where i and j are sibling nodes in \mathcal{T} (denoted $j = \text{sig}(i)$) with the corresponding
 377 index sets \mathcal{I}_i and \mathcal{I}_j in A , respectively. As in Section 3.1, we suppose each node i is
 378 associated with a set of points $\mathbf{x}_i \in \mathbf{s}$.

379 2. Then we write the \tilde{U}, \tilde{V} basis matrices in nested forms. That is, we obtain the \tilde{R}, \tilde{W}
 380 generators in (3.13).

381 The two steps above will be elaborated in Sections 3.3 and 3.4, respectively. The HSS
 382 representations for $\hat{A}^{(F)}$ and $A^{(N)}$ will be merged to form an HSS representation for \hat{A} in
 383 Section 3.5.

384 **3.3. Low-rank forms of off-diagonal blocks of $\hat{A}^{(F)}$.** For sibling nodes i, j of \mathcal{T} , we
 385 find the HSS generators $\tilde{U}_i, \tilde{B}_i, \tilde{V}_j$ so as to write $\hat{A}^{(F)}|_{\mathcal{I}_i \times \mathcal{I}_j}$ in the form of (3.15).

386 The FMM procedure yields a partition that accounts for all far-field interactions between
 387 subsets of \mathbf{x}_i and $\mathbf{s} \setminus \mathbf{x}_i$. Accordingly, \mathcal{I}_i is partitioned into subsets following the partitioning
 388 of \mathbf{x}_i . Later for convenience, we consider the partition of the index set \mathcal{I}_i instead of \mathbf{x}_i . Note
 389 that subsets resulting from the partitioning of \mathcal{I}_i correspond to the descendants of the node i in
 390 \mathcal{T} . Figure 3.4 illustrates the partitioning of \mathcal{I}_i and the subsets correspond to the nodes marked
 391 in Figure 3.5. These nodes form a set which we call the *partition list* associated with i .

392 **DEFINITION 3.2.** Suppose \mathcal{T} is a postordered full binary tree. Let \mathbf{c}_1 and \mathbf{c}_β be the
 393 leftmost and rightmost leaf descendants of a node i , respectively. Let \mathcal{P}_1 be the set of all the
 394 nodes in the path from $\text{par}(\mathbf{c}_1)$ (the parent of \mathbf{c}_1) to the left child of i and \mathcal{P}_2 be the set of all
 395 the nodes in the path from $\text{par}(\mathbf{c}_\beta)$ to the right child of i . Then the partition list associated
 396 with i of \mathcal{T} is

$$\Omega_i = \{\mathbf{c}_1\} \cup \{\text{the right child of each } \mathbf{j} \in \mathcal{P}_1\} \cup \{\text{the left child of each } \mathbf{j} \in \mathcal{P}_2\} \cup \{\mathbf{c}_\beta\}.$$

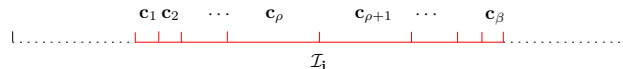


FIG. 3.4. Partitioning of the index set \mathcal{I}_i associated with node i .

397 Thus, Ω_i consists of nodes \mathbf{c}_1 and \mathbf{c}_β corresponding to the boundaries of \mathcal{I}_i and nodes at
 398 levels as high as possible for the interior subsets of \mathcal{I}_i . When we study the interaction between

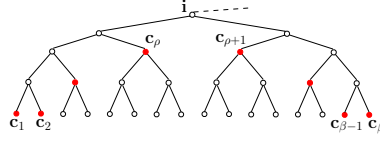


FIG. 3.5. Nodes in the partition list Ω_i (marked as red solid nodes) corresponding to the partition of \mathcal{I}_i in Figure 3.4.

399 i and other nodes, Ω_i is used to provide a way to systematically organize the partition of \mathcal{I}_i .
 400 The resulting partition like in Figure 3.4 is also used in [7].

401 We then find \tilde{U}_i , \tilde{V}_j , and \tilde{B}_i in (3.15). The FMM procedure yields a partition of $\mathcal{I}_i \cup \mathcal{I}_j$,
 402 leading to a blockwise agglomeration [21] of $\hat{A}^{(F)}|_{\mathcal{I}_i \times \mathcal{I}_j}$. For convenience, suppose Ω_i has
 403 the following form as marked in Figures 3.4–3.5:

$$(3.16) \quad \Omega_i = \{\mathbf{c}_1, \mathbf{c}_2, \dots, \mathbf{c}_\rho, \mathbf{c}_{\rho+1}, \dots, \mathbf{c}_\beta\},$$

404 where \mathbf{c}_ρ and $\mathbf{c}_{\rho+1}$ are the left and right children of i , respectively. Similarly, suppose Ω_j has
 405 the following form:

$$(3.17) \quad \Omega_j = \{\mathbf{d}_1, \mathbf{d}_2, \dots, \mathbf{d}_\xi, \mathbf{d}_{\xi+1}, \dots, \mathbf{d}_\theta\}.$$

406 where \mathbf{d}_ξ and $\mathbf{d}_{\xi+1}$ are the left and right children of j , respectively. As shown in Section 3.1.1,
 407 for each pair of separated sets \mathbf{c}_i and \mathbf{d}_j , we can find a low-rank form

$$(3.18) \quad \hat{A}^{(F)}|_{\mathcal{I}_{\mathbf{c}_i} \times \mathcal{I}_{\mathbf{d}_j}} = \hat{U}_{\mathbf{c}_i} \hat{B}_{\mathbf{c}_i, \mathbf{d}_j} \hat{V}_{\mathbf{d}_j}^T.$$

Note that $\hat{A}^{(F)}|_{\mathcal{I}_{\mathbf{c}_i} \times \mathcal{I}_{\mathbf{d}_j}} = 0$ if \mathbf{c}_i and \mathbf{d}_j are near neighbors. In such a case, we can set $\hat{B}_{\mathbf{c}_i, \mathbf{d}_j} = 0$ so that (3.18) still holds. Then we can assemble all the blocks $\hat{A}^{(F)}|_{\mathcal{I}_{\mathbf{c}_i} \times \mathcal{I}_{\mathbf{d}_j}}$ for $i = 1, \dots, \beta, j = 1, \dots, \theta$ into $\tilde{U}_i \tilde{B}_i \tilde{V}_j^T$ in (3.15), where

$$(3.19) \quad \tilde{U}_i = \text{diag}(\hat{U}_{\mathbf{c}_1}, \dots, \hat{U}_{\mathbf{c}_\beta}), \quad \tilde{V}_j = \text{diag}(\hat{V}_{\mathbf{d}_1}, \dots, \hat{V}_{\mathbf{d}_\theta}),$$

$$(3.20) \quad \tilde{B}_i = \begin{bmatrix} \hat{B}_{\mathbf{c}_1, \mathbf{d}_1} & \dots & \hat{B}_{\mathbf{c}_1, \mathbf{d}_\theta} \\ \vdots & \dots & \vdots \\ \hat{B}_{\mathbf{c}_\beta, \mathbf{d}_1} & \dots & \hat{B}_{\mathbf{c}_\beta, \mathbf{d}_\theta} \end{bmatrix}.$$

408 An illustration of (3.15) with (3.19)–(3.20) is shown in Figure 3.6.

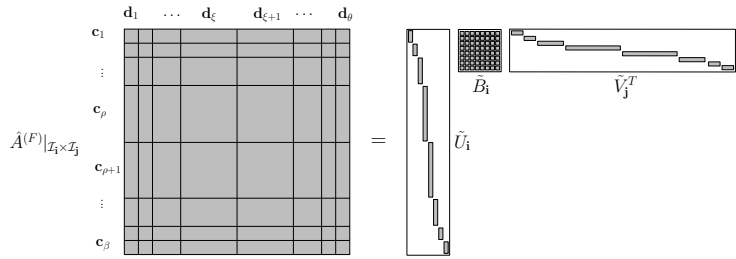


FIG. 3.6. Illustration of (3.15) with (3.19)–(3.20) for the low-rank form of $\hat{A}^{(F)}|_{\mathcal{I}_i \times \mathcal{I}_j}$, where $j = \text{sib}(i)$.

409 **3.4. Nested \tilde{U}, \tilde{V} basis matrices.** We then derive the nested forms of the basis matrices.
 410 Suppose \mathbf{i} and \mathbf{j} are a pair of sibling nodes with parent $\mathbf{p} = \text{par}(\mathbf{i})$. Suppose the partition lists
 411 $\Omega_{\mathbf{i}}$ and $\Omega_{\mathbf{j}}$ associated with \mathbf{i} and \mathbf{j} are in (3.16) and (3.17), respectively, which are used for the
 412 partitioning of the corresponding index sets $\mathcal{I}_{\mathbf{i}}$ and $\mathcal{I}_{\mathbf{j}}$. Let the index set associated with \mathbf{p} in
 413 A be $\mathcal{I}_{\mathbf{p}} = \mathcal{I}_{\mathbf{i}} \cup \mathcal{I}_{\mathbf{j}}$. Then the partition list $\Omega_{\mathbf{p}}$ associated with \mathbf{p} can be obtained by merging
 414 and modifying $\Omega_{\mathbf{i}}$ and $\Omega_{\mathbf{j}}$. This is illustrated in Figure 3.7. We can then let

$$\Omega_{\mathbf{p}} = \{\mathbf{c}_1, \mathbf{c}_2, \dots, \mathbf{c}_{\rho}, \mathbf{e}_1, \mathbf{e}_2, \mathbf{d}_{\xi+1}, \dots, \mathbf{d}_{\theta}\},$$

415 where $\mathbf{e}_1 = \text{par}(\mathbf{c}_{\rho+1})$ and $\mathbf{e}_2 = \text{par}(\mathbf{d}_{\xi})$. Note that the nodes $\mathbf{c}_{\rho+1}, \dots, \mathbf{c}_{\beta}$ are descendants
 416 of \mathbf{e}_1 and $\mathbf{d}_1, \dots, \mathbf{d}_{\xi}$ are descendants of \mathbf{e}_2 .

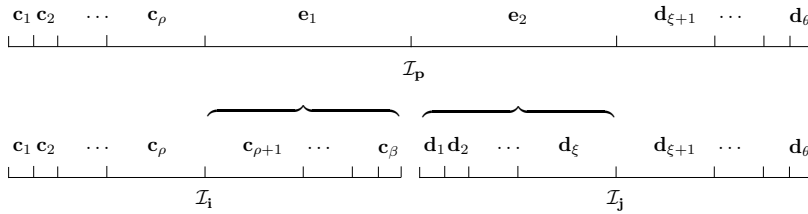


FIG. 3.7. Merging the partitions of $\mathcal{I}_{\mathbf{i}}$ and $\mathcal{I}_{\mathbf{j}}$ to form the partition of $\mathcal{I}_{\mathbf{p}}$.

417 Like in (3.19), we have

$$\tilde{U}_{\mathbf{p}} = \text{diag}(\hat{U}_{\mathbf{c}_1}, \dots, \hat{U}_{\mathbf{c}_{\rho}}, \hat{U}_{\mathbf{e}_1}, \hat{U}_{\mathbf{e}_2}, \hat{U}_{\mathbf{d}_{\xi+1}}, \dots, \hat{U}_{\mathbf{d}_{\theta}}).$$

418 From the translation relations like in (2.24) and (3.8) and noticing Remark 3.1, $\hat{U}_{\mathbf{e}_1}$ and $\hat{U}_{\mathbf{e}_2}$
 419 satisfy

$$\hat{U}_{\mathbf{e}_1} = \text{diag}(\hat{U}_{\mathbf{c}_{\rho+1}} T_{\mathbf{c}_{\rho+1}, \mathbf{e}_1}, \dots, \hat{U}_{\mathbf{c}_{\beta}} T_{\mathbf{c}_{\beta}, \mathbf{e}_1}), \quad \hat{U}_{\mathbf{e}_2} = \text{diag}(\hat{U}_{\mathbf{d}_1} T_{\mathbf{d}_1, \mathbf{e}_2}, \dots, \hat{U}_{\mathbf{d}_{\xi}} T_{\mathbf{d}_{\xi}, \mathbf{e}_2}),$$

where the translation matrices $T_{\mathbf{c}, \mathbf{e}_1}, T_{\mathbf{d}, \mathbf{e}_2}$ are defined like in (2.25). Then

$$\begin{aligned} \tilde{U}_{\mathbf{p}} &= \text{diag}(\hat{U}_{\mathbf{c}_1}, \dots, \hat{U}_{\mathbf{c}_{\rho}}, \hat{U}_{\mathbf{c}_{\rho+1}} T_{\mathbf{c}_{\rho+1}, \mathbf{e}_1}, \dots, \hat{U}_{\mathbf{c}_{\beta}} T_{\mathbf{c}_{\beta}, \mathbf{e}_1}, \\ &\quad \hat{U}_{\mathbf{d}_1} T_{\mathbf{d}_1, \mathbf{e}_2}, \dots, \hat{U}_{\mathbf{d}_{\xi}} T_{\mathbf{d}_{\xi}, \mathbf{e}_2}, \hat{U}_{\mathbf{d}_{\xi+1}}, \dots, \hat{U}_{\mathbf{d}_{\theta}}) \\ &= \text{diag}(\tilde{U}_{\mathbf{i}} \tilde{R}_{\mathbf{i}}, \tilde{U}_{\mathbf{j}} \tilde{R}_{\mathbf{j}}), \end{aligned}$$

420 where

$$(3.21) \quad \tilde{R}_{\mathbf{i}} = \begin{bmatrix} \text{diag} \left(I, \begin{bmatrix} T_{\mathbf{c}_{\rho+1}, \mathbf{e}_1} \\ \vdots \\ T_{\mathbf{c}_{\beta}, \mathbf{e}_1} \end{bmatrix} \right) & 0 \end{bmatrix}, \quad \tilde{R}_{\mathbf{j}} = \begin{bmatrix} 0 & \text{diag} \left(\begin{bmatrix} T_{\mathbf{d}_1, \mathbf{e}_2} \\ \vdots \\ T_{\mathbf{d}_{\xi}, \mathbf{e}_2} \end{bmatrix}, I \right) \end{bmatrix}.$$

421 Here, the zero blocks are chosen to make $\tilde{R}_{\mathbf{i}}$ and $\tilde{R}_{\mathbf{j}}$ have the same column size as $\tilde{U}_{\mathbf{p}}$. Then
 422 we get the nested basis relationship

$$(3.22) \quad \tilde{U}_{\mathbf{p}} = \begin{bmatrix} \tilde{U}_{\mathbf{i}} & \tilde{R}_{\mathbf{i}} \\ \tilde{U}_{\mathbf{j}} & \tilde{R}_{\mathbf{j}} \end{bmatrix}.$$

423 This yields the nested relation for the \tilde{U} basis matrices. We can similarly derive a nested basis
 424 relationship for $\tilde{V}_{\mathbf{i}}$. Since the translation matrices only depend on relevant centers of subsets,

425 \tilde{R}_i and \tilde{W}_i are only determined by the partition of \mathcal{I}_i and are independent of the actual points
 426 in \mathcal{I}_i . It follows that the HSS generator

$$(3.23) \quad \tilde{W}_i = \tilde{R}_i.$$

427 At this point, we obtain all the $\tilde{U}, \tilde{V}, \tilde{R}, \tilde{W}, \tilde{B}$ generators for $\hat{A}^{(F)}$. The \tilde{D} generators of
 428 $\hat{A}^{(F)}$ are zero blocks. Clearly, the generators have block structures that can be explored to
 429 save storage and computational costs.

430 **3.5. HSS representation for \hat{A} .** We then write an HSS representation for $A^{(N)}$ so as to
 431 get an HSS form for $A = \hat{A}^{(F)} + A^{(N)}$. $A^{(N)}$ is a block banded matrix. Suppose $A^{(F)}$ and
 432 $A^{(N)}$ are partitioned conformably. Then the HSS form of $A^{(N)}$ can be explicitly written as
 433 [36]:

$$(3.24) \quad \begin{aligned} \check{U}_i &= I, \quad \check{V}_i = I, \quad \text{for a leaf } i, \\ \check{R}_i &= \begin{cases} [I \ 0] & \text{if } i \text{ is a leaf and } i < \text{sib}(i), \\ [0 \ I] & \text{if } i \text{ is a leaf and } i > \text{sib}(i), \\ \text{diag}(I, 0), & \text{if } i \text{ is a nonleaf node and } i < \text{sib}(i), \\ \text{diag}(0, I), & \text{if } i \text{ is a nonleaf node and } i > \text{sib}(i), \end{cases} \\ \check{W}_i &: \text{ in the same form as } \check{R}_i, \\ \check{B}_i &= \begin{cases} A|_{\mathcal{I}_i \times \mathcal{I}_{\text{sib}(i)}}, & \text{if } i \text{ is a leaf and } i < \text{sib}(i), \\ A|_{\mathcal{I}_{\text{sib}(i)} \times \mathcal{I}_i}, & \text{if } i \text{ is a leaf and } i > \text{sib}(i), \\ \begin{bmatrix} & 0 \\ A|_{\mathcal{I}_i \times \mathcal{I}_{\text{sib}(i)}} & \end{bmatrix}, & \text{if } i \text{ is a nonleaf node and } i < \text{sib}(i), \\ \begin{bmatrix} & A|_{\mathcal{I}_{\text{sib}(i)} \times \mathcal{I}_i} \\ 0 & \end{bmatrix}, & \text{if } i \text{ is a nonleaf node and } i > \text{sib}(i). \end{cases} \end{aligned}$$

With the HSS generators for $A^{(F)}$ and $A^{(N)}$ at hand, it is easy to verify (see, e.g., [36]) that the HSS generators for \hat{A} are given by:

$$(3.25) \quad \begin{aligned} D_i &= \tilde{D}_i + \check{D}_i, \quad B_i = \text{diag}(\tilde{B}_i, \check{B}_i), \\ U_i &= [\tilde{U}_i \ \check{U}_i], \quad V_i = [\tilde{V}_i \ \check{V}_i], \\ R_i &= \text{diag}(\tilde{R}_i, \check{R}_i), \quad W_i = \text{diag}(\tilde{W}_i, \check{W}_i). \end{aligned}$$

434 Due to the summation, the sizes of some generators such as B_i may be larger than necessary.
 435 If a more compact HSS form is desired, a recompression step may be applied like in some
 436 other HSS methods [9, 14, 37].

437 It can be shown that the cost to construct the HSS matrix is also $\mathcal{O}(rn)$. The ULV
 438 factorization of the resulting HSS form costs $\mathcal{O}(r^2n)$.

439 **REMARK 3.3.** Here in the 1D case, both the FMM and the HSS forms use binary trees.
 440 For 2D problems, quad-trees are typically used for the FMM. If there is a need to convert
 441 a 2D FMM matrix to an HSS form, we may re-derive the FMM matrix form based on the
 442 repeated bisection of the domain so as to generate a binary tree structure. Then the conversion
 443 to an HSS form can follow a procedure similar to the 1D case, by agglomerating low-rank
 444 subblocks to form an approximation to an off-diagonal block. However, there will be a lot
 445 more such subblocks (as many as $\mathcal{O}(\sqrt{n})$) than the 1D case (at most $\mathcal{O}(\log n)$). The maximum
 446 off-diagonal rank in the HSS form will be as high as $\mathcal{O}(\sqrt{n})$. This makes the resulting HSS
 447 form less attractive than the 1D case. In three dimensions, the off-diagonal rank will be even
 448 higher.

449 **3.6. Norm bounds of generators and additional stability discussions.** Now we would
 450 like to briefly illustrate that the structured representations given in the previous sections satisfy
 451 some stability requirements of computations such as matrix-vector multiplications (with the
 452 FMM or HSS form) and ULV factorizations (with the HSS form). The backward stability of
 453 several commonly used HSS algorithms has been studied in [7, 34, 35], where the stability
 454 analysis essentially relies on the following conditions.

455 • The U, V generators have bounded norms.
 456 • The B generators have norms bounded by a small constant multiple of the norm of
 457 A .

458 Thus, our purpose is to show that, the FMM and HSS generators we obtain using our
 459 stabilization strategy satisfy such norm requirements. Based on the analysis in Section 2, we
 460 have the following bounds for the norms of the FMM and HSS generators.

COROLLARY 3.4. *Suppose (2.26) holds for any descendant \mathbf{c} of a nonleaf node \mathbf{i} in \mathcal{T} . Then for the approximation \hat{A} to A in (1.2) with (2.2) and $\tau \in (0, \frac{4}{5})$, the FMM generators $\hat{U}, \hat{V}, \hat{B}$ in (2.17) and \hat{R}, \hat{W} in (3.8) satisfy*

$$\begin{aligned} \|\hat{U}\|_{\max} &\leq 1, \quad \|\hat{V}\|_{\max} \leq 1, \quad \|\hat{R}\|_{\max} \leq 1, \quad \|\hat{W}\|_{\max} \leq 1, \\ \|\hat{B}\|_{\max} &\leq \max\{1, 3\tau\}(1 + \tau)\|A\|_{\max}. \end{aligned}$$

The HSS generators U, V, R, W, B in (3.25) satisfy

$$\begin{aligned} \|U\|_{\max} &\leq 1, \quad \|V\|_{\max} \leq 1, \quad \|R\|_{\max} \leq 1, \quad \|W\|_{\max} \leq 1, \\ \|B\|_{\max} &\leq \max\{1, 3\tau\}(1 + \tau)\|A\|_{\max}. \end{aligned}$$

461 *Proof.* The max-norm results for the generators $\hat{U}, \hat{V}, \hat{R}, \hat{W}$ are immediate from Theorems
 462 2.5 and 2.7. When $\hat{A}|_{\mathcal{I}_i \times \mathcal{I}_j} = \hat{U}_i \hat{B}_{i,j} \hat{V}_j^T$ like in (3.2) for two separated point sets \mathbf{x}_i and \mathbf{x}_j ,
 463 we can use Theorem 2.5 and the derivation like in the proof for Theorem 2.9 to get

$$(3.26) \quad \|\hat{B}_{i,j}\|_{\max} \leq \max\{1, 3\tau\}(1 + \tau)\|A|_{\mathcal{I}_i \times \mathcal{I}_j}\|_{\max} \leq \max\{1, 3\tau\}(1 + \tau)\|A\|_{\max}.$$

Next, it is clear from (3.24) that the HSS generators $\check{U}, \check{V}, \check{R}, \check{W}$ for $\hat{A}^{(N)}$ have entrywise magnitudes bounded by 1. Then it can be seen from (3.25) that the HSS generators U, V, R, W for \hat{A} have entrywise magnitudes bounded by 1. The HSS generators \tilde{B} like in (3.20) also satisfy the bound in (3.26). Then

$$\begin{aligned} \|B\|_{\max} &\leq \max\{\|\tilde{B}\|_{\max}, \|\check{B}\|_{\max}\} \leq \max\{\max\{1, 3\tau\}(1 + \tau)\|A\|_{\max}, \|A\|_{\max}\} \\ &\leq \max\{1, 3\tau\}(1 + \tau)\|A\|_{\max}. \end{aligned}$$

464 We thus get the bound for $\|B\|_{\max}$. □

465 Based on these norm bounds and the stability study in Section 2.5, the stability of the
 466 overall FMM algorithm and the HSS matrix-vector multiplication can be naturally shown.
 467 The stability analysis is similar to that in [34]. In fact, such stability can be conveniently
 468 understood based on the telescoping expansions in (3.11) and (3.14). The stability of ULV
 469 factorizations and solutions for the HSS form of \hat{A} can be shown similarly to the work in
 470 [34, 35]. The actual derivations involve lengthy technical details and thus the readers are
 471 referred to [34, 35].

4. Numerical tests. Here, we use some numerical examples to demonstrate the performance of our techniques and support the analysis. We show how our stable FMM/HSS constructions with the scaling strategy control the norms of the generators and the approximation accuracy. We also test the accuracy of direct solution. Different types of kernels as

follows are tested:

$$(4.1) \quad \kappa_1(x, y) = \begin{cases} \frac{1}{x-y}, & \text{if } x \neq y, \\ 1, & \text{otherwise,} \end{cases}$$

$$(4.2) \quad \kappa_2(x, y) = \begin{cases} \frac{1}{(x-y)^2}, & \text{if } x \neq y, \\ 1, & \text{otherwise,} \end{cases} \quad \kappa_3(x, y) = \begin{cases} \log|x-y|, & \text{if } x \neq y, \\ 1, & \text{otherwise.} \end{cases}$$

472 To account for factors like the scale and distribution of point sets, the kernels are evaluated
 473 at various 1D and 2D point sets.

- 474 • Set s_1 : A set of uniform grid points in $[0, 1]$.
- 475 • Set s_2 : A set of randomly generated points in $[0, 1]$.
- 476 • Set s_3 : A set of points on the boundary curve of a stingray shape defined by coordi-
 477 nates

$$\left(40 \sin \frac{(2i-1)\pi}{n} + 40 \cos^4 \frac{2(2i-1)\pi}{n}, 40 \cos^5 \frac{(2i-1)\pi}{n} \right), \quad i = 1, 2, \dots, n.$$

478 See Figure 4.1(a) for an illustration.

- 479 • Set s_4 : A set of uniform grid points in $[0, 400] \times [0, 400]$.
- 480 • Set s_5 : A set of randomly generated points in $[0, 400] \times [0, 400]$. See Figure 4.1(b)
 481 for an example.

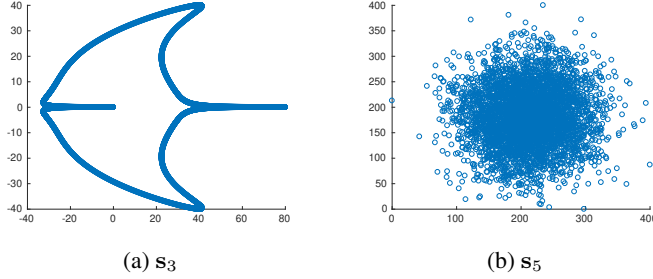


FIG. 4.1. Illustration of points in examples of s_3 and s_5 .

482 To generate a binary tree \mathcal{T} for the FMM/HSS matrix construction, we hierarchically
 483 bisect each set. Separated subsets are adaptively identified in the partitioning process.

484 **4.1. Entrywise magnitudes of generators.** We illustrate the benefit of the proposed
 485 stable FMM/HSS matrix construction by investigating the entrywise magnitudes of the genera-
 486 tors with and without applying the scaling strategy (denoted **New** and **Unscaled** in the tests,
 487 respectively). According to (3.25) and Corollary 3.4, we just need to report the entrywise
 488 magnitudes for the HSS version since the results are almost the same for the FMM case. To
 489 inspect how **New** differs from **Unscaled**, we report the entrywise magnitudes of the HSS
 490 generators of $\tilde{A}^{(F)}$ as follows:

$$(4.3) \quad \mathcal{B} \equiv \max_{i \in \mathcal{T}} \|\tilde{B}_i\|_{\max}, \quad \mathcal{U} \equiv \max_{i \in \mathcal{T}} \|\tilde{U}_i\|_{\max}, \quad \mathcal{R} \equiv \max_{i \in \mathcal{T}} \|\tilde{R}_i\|_{\max}.$$

491 Results for the generators \tilde{V} and \tilde{W} are not shown since they are similar to those for \tilde{U} and \tilde{R} ,
 492 respectively.

493 We pick the number of points in each point set (or the order of A) as $n = 4096$ and set
 494 each leaf level partition to include at most 256 points. The separation ration τ in Definition 2.1

495 is set to be $\frac{1}{2}$ for sets $\mathbf{s}_1, \mathbf{s}_2$ and $\frac{\sqrt{2}}{2}$ for $\mathbf{s}_3, \mathbf{s}_4, \mathbf{s}_5$. The number of expansion terms r increases
 496 from 5 to 30 so as to show how the standard Taylor series expansion leads to large entrywise
 497 magnitudes of the generators.

498 For the kernel $\kappa_1(x, y)$ in (4.1), the results on the maximum entrywise magnitudes (4.3)
 499 are given in Tables 4.1 and 4.2. As r increases, the maximum entrywise magnitudes of some
 500 generators from **Unscaled** get quite large. For some cases, even a small increase in r leads to
 501 a rapid increase in the entrywise magnitudes and the magnitudes become significantly larger
 502 than $\|A\|_{\max}$. Such large magnitudes occur in different generators, depending on the point
 503 set. On the other hand, **New** fully resolves this issue and produces generators with uniformly
 504 bounded matrix entries regardless of the scale and the distribution of the point sets. That is, all
 505 \mathcal{U}, \mathcal{R} are bounded by 1, which is consistent with Corollary 3.4. The \mathcal{B} values are also bounded
 506 by modest constants.

TABLE 4.1
*Maximum entrywise magnitudes of the HSS generators of $\hat{A}^{(F)}$ obtained with **Unscaled** and **New** for $\kappa_1(x, y)$
 discretized on the sets $\mathbf{s}_1, \mathbf{s}_2$.*

Set	$\ A\ _{\max}$	r	Unscaled		New	
			\mathcal{B}	$\max\{\mathcal{U}, \mathcal{R}\}$	\mathcal{B}	$\max\{\mathcal{U}, \mathcal{R}\}$
\mathbf{s}_1	$4.10e3$	5	$1.04e05$	1.00	$5.33e00$	1.00
		10	$6.77e12$	1.00	$5.33e00$	1.00
		15	$7.03e21$	1.00	$5.33e00$	1.00
		20	$4.24e31$	1.00	$5.33e00$	1.00
		25	$9.34e41$	1.00	$5.33e00$	1.00
		30	$5.75e52$	1.00	$5.33e00$	1.00
\mathbf{s}_2	$3.60e7$	5	$1.06e08$	1.00	$2.13e01$	1.00
		10	$7.09e18$	1.00	$2.13e01$	1.00
		15	$7.52e30$	1.00	$2.13e01$	1.00
		20	$4.64e43$	1.00	$2.13e01$	1.00
		25	$1.05e57$	1.00	$2.13e01$	1.00
		30	$6.58e70$	1.00	$2.13e01$	1.00

507 Similar results can also be observed for other kernel functions. We repeat some tests with
 508 the kernels $\kappa_2(x, y)$ and $\kappa_3(x, y)$ in (4.2). The results are shown in Table 4.3. Again, while
 509 some generators from **Unscaled** have large magnitudes, the generators from **New** always
 510 have well-controlled entrywise magnitudes.

511 Other than increasing r , another way to demonstrate the advantage of **New** over **Unscaled**
 512 is to increase the number of points n in a set while keeping the points still within the given
 513 interval. In this way, the points get more clustered and the entries in (2.9) and (2.12) used in
 514 **Unscaled** get larger. For example, for $\kappa_1(x, y)$ discretized on \mathbf{s}_2 , we fix $r = 20$ and increase
 515 n . The \mathcal{B} magnitudes are plotted in Figure 4.2. It can be observed that \mathcal{B} from **Unscaled**
 516 increases quickly with n , while it remains well bounded from **New**. We can observe similar
 517 comparisons for the other sets and kernels.

518 REMARK 4.1. In practice, even if r is very small (say, smaller than 10), **Unscaled**
 519 may still provide generators with huge entries that pose stability risks. Also, we have used
 520 computational domains with different sizes to show that **Unscaled** is susceptible to problem
 521 settings but **New** is much more robust.

522 **4.2. Accuracy and efficiency.** The large magnitudes of the entries of the generators can
 523 cause accuracy loss to structured algorithms using the generators. To demonstrate this, we
 524 perform some operations on the generators in (3.25). The recompression step mentioned

TABLE 4.2
*Maximum entrywise magnitudes of the HSS generators of $\hat{A}^{(F)}$ obtained with **Unscaled** and **New** for $\kappa_1(x, y)$ discretized on the sets $\mathbf{s}_3, \mathbf{s}_4, \mathbf{s}_5$.*

Set	$\ A\ _{\max}$	r	Unscaled			New	
			\mathcal{B}	\mathcal{U}	\mathcal{R}	\mathcal{B}	$\max\{\mathcal{U}, \mathcal{R}\}$
\mathbf{s}_3	$4.71e13$	5	$2.35e - 02$	$1.49e04$	$1.96e02$	$2.35e - 02$	1.00
		10	$2.35e - 02$	$8.59e06$	$5.49e02$	$2.69e - 02$	1.00
		15	$2.35e - 02$	$3.12e08$	$5.49e02$	$3.00e - 02$	1.00
		20	$2.35e - 02$	$1.95e09$	$5.49e02$	$3.20e - 02$	1.00
		25	$2.35e - 02$	$3.34e09$	$5.49e02$	$3.32e - 02$	1.00
		30	$2.35e - 02$	$3.34e09$	$5.49e02$	$3.42e - 02$	1.00
\mathbf{s}_4	1.00	5	$3.59e - 03$	$9.78e05$	1.00	$3.59e - 03$	1.00
		10	$3.59e - 03$	$1.06e11$	1.00	$4.39e - 03$	1.00
		15	$3.59e - 03$	$7.19e14$	1.00	$4.90e - 03$	1.00
		20	$3.59e - 03$	$8.42e17$	1.00	$5.21e - 03$	1.00
		25	$3.59e - 03$	$2.70e20$	1.00	$5.42e - 03$	1.00
		30	$3.59e - 03$	$3.09e22$	1.00	$5.57e - 03$	1.00
\mathbf{s}_5	2.98e1	5	$9.30e - 03$	$5.90e06$	1.00	$9.30e - 03$	1.00
		10	$9.30e - 03$	$6.02e12$	1.00	$1.09e - 02$	1.00
		15	$9.30e - 03$	$3.86e17$	1.00	$1.22e - 02$	1.00
		20	$9.30e - 03$	$4.27e21$	1.00	$1.30e - 02$	1.00
		25	$9.30e - 03$	$1.29e25$	1.00	$1.35e - 02$	1.00
		30	$9.30e - 03$	$1.40e28$	1.00	$1.39e - 02$	1.00

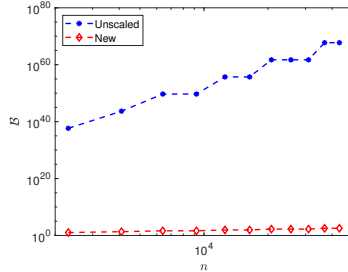


FIG. 4.2. Maximum entrywise magnitude \mathcal{B} in (4.3) from **Unscaled** and **New** for $\hat{A}^{(F)}$ with $\kappa_1(x, y)$ discretized on \mathbf{s}_2 of different sizes n .

525 after (3.25) is first applied with the full machine precision as the tolerance so as to avoid
 526 introducing extra approximation errors. The resulting generators are used for matrix-vector
 527 multiplications and linear system solutions via ULV factorizations and solutions. Without
 528 the recompression, the unscaled version can sometimes give reasonable accuracies in matrix-
 529 vector multiplications. However, it is quite sensitive to more complicated operations such as
 530 recompression. In addition, it can encounter overflow for larger ranks.

531 For each matrix-vector multiplication, we generate a random vector w and multiply the
 532 approximate matrix with w to get a vector \hat{b} , which approximates the exact vector $b = Aw$.
 533 For $\kappa_1(x, y)$ discretized on the point sets as above, the resulting matrix-vector multiplication
 534 errors $\frac{\|\hat{b} - b\|_1}{\|b\|_1}$ are shown in Table 4.4. In exact arithmetic, when r increases, the approximate
 535 matrix gets more accurate and the error $\frac{\|\hat{b} - b\|_1}{\|b\|_1}$ should decrease. However, with **Unscaled**,
 536 only modest accuracies are achieved. Specifically for the sets $\mathbf{s}_1, \mathbf{s}_2$, the accuracy in Table

TABLE 4.3

Maximum entrywise magnitudes of the HSS generators of $\hat{A}^{(F)}$ obtained with **Unscaled** and **New** for the kernels in (4.2) discretized on the sets $\mathbf{s}_2, \mathbf{s}_5$.

Kernel	Set	$\ A\ _{\max}$	r	Unscaled		New		
				\mathcal{B}	$\max\{\mathcal{U}, \mathcal{R}\}$	\mathcal{B}	$\max\{\mathcal{U}, \mathcal{R}\}$	
$\kappa_2(x, y)$	\mathbf{s}_2	$1.30e15$	5	$1.13e10$	1.00	$5.63e02$	1.00	
			10	$1.51e21$	1.00	$7.41e02$	1.00	
			15	$2.41e33$	1.00	$8.28e02$	1.00	
			20	$1.98e46$	1.00	$8.80e02$	1.00	
			25	$5.57e59$	1.00	$9.16e02$	1.00	
			30	$4.21e73$	1.00	$9.41e02$	1.00	
	\mathbf{s}_5	$8.90e02$	5	$8.65e-05$	$5.90e06$	1.00	$2.22e-04$	1.00
			10	$8.65e-05$	$6.02e12$	1.00	$2.93e-04$	1.00
			15	$8.65e-05$	$3.86e17$	1.00	$3.33e-04$	1.00
			20	$8.65e-05$	$4.27e21$	1.00	$3.65e-04$	1.00
			25	$8.65e-05$	$1.29e25$	1.00	$3.87e-04$	1.00
			30	$8.65e-05$	$1.40e28$	1.00	$4.03e-04$	1.00
$\kappa_3(x, y)$	\mathbf{s}_2	$1.74e01$	5	$1.24e06$	1.00	3.06	1.00	
			10	$3.69e16$	1.00	3.06	1.00	
			15	$2.52e28$	1.00	3.06	1.00	
			20	$1.14e41$	1.00	3.06	1.00	
			25	$2.04e54$	1.00	3.06	1.00	
			30	$1.06e68$	1.00	3.06	1.00	
	\mathbf{s}_5	$8.90e02$	5	5.76	$5.90e06$	1.00	5.76	1.00
			10	5.76	$6.02e12$	1.00	5.76	1.00
			15	5.76	$3.86e17$	1.00	5.76	1.00
			20	5.76	$4.27e21$	1.00	5.76	1.00
			25	5.76	$1.29e25$	1.00	5.76	1.00
			30	5.76	$1.40e28$	1.00	5.76	1.00

537 4.4 does not improve much for increasing r . For the sets $\mathbf{s}_3, \mathbf{s}_4, \mathbf{s}_5$, the accuracy in Table 4.4
 538 initially improves with increasing r but then decreases. On the other hand, such situations
 539 do not occur with **New**. For all the sets, the accuracy increases with r to near the machine
 540 precision.

541 For the kernels $\kappa_2(x, y)$ and $\kappa_3(x, y)$, the results are given in Table 4.5.

542 We then fix $r = 20$ and increase n . Figure 4.3(a) shows the relative errors of the matrix-
 543 vector multiplications for one case. Much higher accuracies are achieved for all n with **New**
 544 than with **Unscaled**.

545 We can similarly compare the accuracies in linear system solution with ULV factorization
 546 and ULV solution. We form the right-hand side vector $b = Aw$ with random w and suppose
 547 \hat{w} is the approximate solution. For $\kappa_1(x, y)$ discretized on the five sets as above, Table 4.6
 548 gives the relative residuals $\frac{\|A\hat{w} - b\|_1}{\|b\|_1}$. With **Unscaled**, only modest accuracies can be achieved
 549 for some cases and very inaccurate results are produced for the other cases. With **New**, the
 550 relative residuals reduce with increasing r to near the machine precision.

551 Similarly, with $r = 20$ and varying n , the accuracy results for one test is given in Figure
 552 4.3(b). While the accuracy with **Unscaled** remains modest and gets worse with increasing n ,
 553 the accuracy with **New** stays high for all the n values.

TABLE 4.4

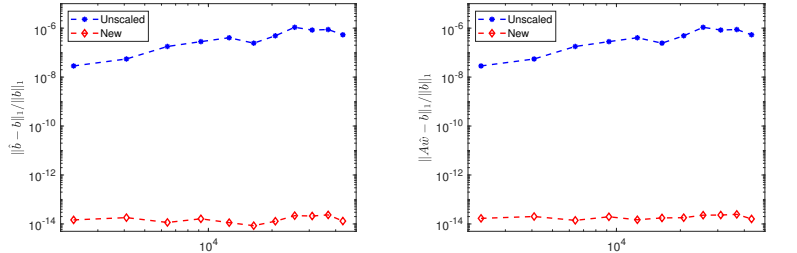
$\frac{\|\hat{b}-b\|_1}{\|b\|_1}$: accuracy of matrix-vector multiplications based on **Unscaled** and **New** with the kernel $\kappa_1(x, y)$.

	r	s₁	s₂	s₃	s₄	s₅
Unscaled	5	7.03e - 06	1.34e - 06	4.13e - 13	1.11e - 04	1.20e - 04
	10	8.30e - 08	5.55e - 08	1.50e - 10	6.32e - 07	6.93e - 07
	15	8.35e - 08	5.50e - 08	1.05e - 08	7.18e - 09	1.98e - 01
	20	8.47e - 08	5.49e - 08	7.24e - 06	2.95e - 01	2.62e - 01
	25	7.61e - 08	5.49e - 08	9.78e - 02	3.21e - 01	2.91e - 01
	30	7.65e - 08	5.49e - 08	2.13e - 01	3.25e - 01	2.99e - 01
New	5	7.03e - 06	1.33e - 06	6.84e - 14	1.11e - 04	1.20e - 04
	10	1.14e - 08	2.67e - 09	1.78e - 14	6.32e - 07	6.93e - 07
	15	2.72e - 11	5.55e - 12	3.26e - 14	7.18e - 09	7.20e - 09
	20	7.84e - 14	1.81e - 14	3.17e - 14	9.93e - 11	1.08e - 10
	25	1.62e - 15	1.83e - 15	2.16e - 14	1.76e - 12	1.92e - 12
	30	1.54e - 15	1.81e - 15	4.60e - 14	3.49e - 14	4.17e - 14

TABLE 4.5

$\frac{\|\hat{b}-b\|_1}{\|b\|_1}$: accuracy of matrix-vector multiplications based on **Unscaled** and **New** with the kernels $\kappa_2(x, y)$ and $\kappa_3(x, y)$.

	r	$\kappa_2(x, y)$		$\kappa_3(x, y)$	
		s₂	s₅	s₂	s₅
Unscaled	5	2.66e - 11	4.40e - 06	1.11e - 04	2.11e - 05
	10	1.26e - 12	4.76e - 08	2.80e - 06	6.07e - 08
	15	1.26e - 12	1.55e - 02	2.80e - 06	5.43e - 01
	20	1.26e - 12	1.94e - 02	2.80e - 06	6.67e - 01
	25	1.26e - 12	1.97e - 02	2.80e - 06	7.14e - 01
	30	1.26e - 12	2.03e - 02	2.80e - 06	6.71e - 01
New	5	2.66e - 11	4.40e - 06	1.11e - 04	2.11e - 05
	10	7.88e - 14	4.76e - 08	9.99e - 08	6.07e - 08
	15	2.14e - 15	7.26e - 10	1.71e - 10	4.22e - 10
	20	1.89e - 15	1.45e - 11	3.60e - 13	4.98e - 12
	25	1.89e - 15	3.16e - 13	3.97e - 15	6.22e - 14
	30	1.89e - 15	9.29e - 15	4.00e - 15	4.14e - 15



(a) $\frac{\|\hat{b}-b\|_1}{\|b\|_1}$ in matrix-vector multiplications (b) $\frac{\|A\hat{w}-b\|_1}{\|b\|_1}$ in linear system solutions

FIG. 4.3. Accuracies of matrix-vector multiplications and linear system solutions based on **Unscaled** and **New** with the kernel $\kappa_1(x, y)$ discretized on **s₂** of different size n .

TABLE 4.6
*Residuals of ULV solutions after ULV factorizations based on **New** with the kernel $\kappa_1(x, y)$.*

	r	s_1	s_2	s_3	s_4	s_5
Unscaled	5	$7.03e - 06$	$1.34e - 06$	$4.75e - 10$	$8.85e - 04$	$2.54e - 04$
	10	$8.30e - 08$	$5.55e - 08$	$3.62e - 07$	$2.47e - 06$	$1.41e - 06$
	15	$8.35e - 08$	$5.50e - 08$	$4.40e - 04$	$1.42e - 08$	$5.34e + 02$
	20	$8.47e - 08$	$5.49e - 08$	$9.20e + 01$	$1.32e + 01$	$4.13e + 02$
	25	$7.61e - 08$	$5.49e - 08$	$3.08e + 10$	$1.36e + 01$	$2.59e + 02$
	30	$7.65e - 08$	$5.49e - 08$	$6.73e + 08$	$2.55e + 01$	$8.92e + 03$
New	5	$7.03e - 06$	$1.33e - 06$	$4.79e - 09$	$8.85e - 04$	$2.54e - 04$
	10	$1.14e - 08$	$2.67e - 09$	$2.10e - 12$	$2.47e - 06$	$1.41e - 06$
	15	$2.72e - 11$	$5.55e - 12$	$1.04e - 12$	$1.42e - 08$	$1.82e - 08$
	20	$7.96e - 14$	$2.01e - 14$	$2.33e - 13$	$2.53e - 10$	$2.22e - 10$
	25	$4.41e - 15$	$6.77e - 15$	$2.93e - 13$	$2.61e - 12$	$2.13e - 12$
	30	$4.90e - 15$	$6.49e - 15$	$4.23e - 13$	$4.83e - 14$	$8.30e - 14$

554 Finally, it is convenient to check the efficiency of relevant structured algorithms. Such
 555 efficiency studies have been done extensively in many existing literatures. Here, we just
 556 use Figure 4.4 with $r = 20$ to show the storage needed for the generators for $\hat{A}^{(F)}$, which
 557 essentially reflects the cost needed to multiply $\hat{A}^{(F)}$ with a vector. The storage in Figure 4.4 is
 558 roughly linear in n .

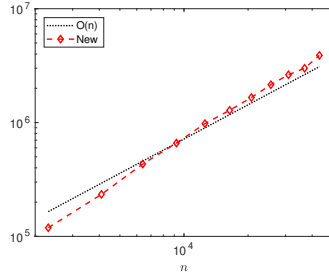


FIG. 4.4. Storage (number of nonzero entries) for the $\tilde{D}, \tilde{U}, \tilde{V}, \tilde{R}, \tilde{W}, \tilde{B}$ generators for $\hat{A}^{(F)}$ from **New** for $\kappa_1(x, y)$ discretized on s_2 with different number of points n .

559 **5. Conclusions.** In this paper, stabilization strategies and backward stability studies are
 560 given for relevant low-rank approximations and translation relations in an intuitive matrix
 561 version of the FMM. An FMM matrix example is also shown, followed by ideas to convert
 562 the FMM matrix into an HSS form that admits stable factorizations. The stable matrix
 563 version FMM employs a scaling strategy to revise the low-rank approximations based on
 564 Taylor expansions for some kernel functions. Rigorous norm bounds are shown for the
 565 FMM and HSS generators. These bounds lead to the backward stability of fast matrix-vector
 566 multiplications with the matrices. The HSS form can be used for stable linear system solution
 567 via ULV factorization and solution.

568 Since the approximation based on Taylor expansions can be substituted by other approxi-
 569 mations such as polynomial interpolations [13, 19, 40], numerical integrations [1, 41], kernel
 570 independent FMM [25, 42, 43], etc., we expect that our ideas can also be generalized to
 571 various other types of FMM. Our stabilization strategies are derived based on 2D point sets,
 572 but can also be extended to higher dimensions. It is convenient to generalize the norm bounds

573 and stability analysis in Sections 2.5 and 3.6. Although we only give the FMM matrix using
 574 one-dimensional sets as an example, the essential ideas can be directly modified for higher
 575 dimensions. Some details will appear in [27].

576

REFERENCES

- 577 [1] C. R. ANDERSON, *An implementation of the fast multipole method without multipoles*, SIAM J. Sci. Stat. Comput., 13 (1992), pp. 923–947.
- 578 [2] S. BÖRM, L. GRASEDYCK, AND W. HACKBUSCH, *Introduction to hierarchical matrices with applications*, Engineering analysis with boundary elements, 27 (2003), pp. 405–422.
- 579 [3] D. CAI, E. CHOW, L. ERLANDSON, Y. SAAD, AND Y. XI, *SMASH: Structured matrix approximation by separation and hierarchy*, Numer. Linear Algebra Appl., 25 (2018).
- 580 [4] D. CAI AND J. XIA, *A stable and efficient matrix version of the fast multipole method*, preprint, <https://www.math.psu.edu/~cai92/fmm2hss.pdf>.
- 581 [5] S. CHANDRASEKARAN, P. DEWILDE, M. GU, W. LYONS, AND T. PALS, *A fast solver for hss representations via sparse matrices*, SIAM J. Matrix Anal. Appl., 29 (2007), pp. 67–81.
- 582 [6] S. CHANDRASEKARAN, M. GU, W. LYONS, *A fast adaptive solver for hierarchically semiseparable representations*, CALCOLO 42 (2005), pp. 171–185.
- 583 [7] S. CHANDRASEKARAN, M. GU, AND T. PALS, *A fast ULV decomposition solver for hierarchically semiseparable representations*, SIAM J. Matrix Anal. Appl., 28 (2006), pp. 603–622.
- 584 [8] S. CHANDRASEKARAN, M. GU, X. SUN, J. XIA, AND J. ZHU, *A superfast algorithm for Toeplitz systems of linear equations*, SIAM J. Matrix Anal. Appl., 29 (2007), pp. 1247–1266.
- 585 [9] E. CORONA, P.-G. MARTINSSON, AND D. ZORIN, *An $O(N)$ direct solver for integral equations on the plane*, Appl. Comput. Harmon. Anal., 38 (2015), pp. 284–317.
- 586 [10] E. DARVE, *The fast multipole method: numerical implementation*, J. Comput. Phys., 160 (2000), pp. 195–240.
- 587 [11] E. DARVE AND P. HAVÉ, *Fast multipole method for Maxwell equations stable at all frequencies*, Phil. Trans. R. Soc. Lond. A (2004) 362, pp. 603–628.
- 588 [12] E. DARVE AND P. HAVÉ, *Efficient fast multipole method for low-frequency scattering*, J. Comput. Phys., (197) 2004, pp. 341–363.
- 589 [13] A. DUTT, M. GU, AND V. ROKHLIN, *Fast algorithms for polynomial interpolation, integration, and differentiation*, SIAM J. Numer. Anal., 33 (1996), pp. 1689–1711.
- 590 [14] A. GILLMAN, *Fast Direct Solvers for Elliptic Partial Differential Equations*, PhD Thesis, University of Colorado at Boulder, 2011.
- 591 [15] Z. GIMBUTAS, N. F. MARSHALL, AND V. ROKHLIN, *A fast simple algorithm for computing the potential of charges on a line*, Appl. Comput. Harmon. Anal., 49 (2020), pp. 815–830.
- 592 [16] L. GREENGARD AND V. ROKHLIN, *A fast algorithm for particle simulations*, J. Comput. Phys., 73 (1987), pp. 325–348.
- 593 [17] L. GREENGARD AND V. ROKHLIN, *On the efficient implementation of the fast multipole algorithm*, Technical report RR-602, Department of Computer Science, Yale University, (1988).
- 594 [18] W. HACKBUSCH AND S. BÖRM, *Data-sparse approximation by adaptive \mathcal{H}^2 -matrices*, Computing, 69 (2002), pp. 1–35.
- 595 [19] W. HACKBUSCH AND S. BÖRM, *\mathcal{H}^2 -matrix approximation of integral operators by interpolation*, Appl. Numer. Math., 43 (2002), pp. 129–143.
- 596 [20] W. HACKBUSCH, B. N. KHOROMSKIJ, AND S. A. SAUTER, *On \mathcal{H}^2 -matrices*, in Lectures on applied mathematics, Hans-Joachim Bungartz, Ronald H. W. Hoppe, and Christoph Zenger, eds., Springer, Berlin, 2000, pp. 9–29.
- 597 [21] W. HACKBUSCH, B. N. KHOROMSKIJ, AND R. KRIEMANN, *Hierarchical matrices based on a weak admissibility criterion*, Computing, 73 (2004), pp. 207–243.
- 598 [22] N. J. HIGHAM, *Accuracy and Stability of Numerical Algorithms*, 2nd ed., SIAM, Philadelphia, 2002.
- 599 [23] X. LIU, J. XIA, AND M. V. DE HOOP, *Parallel randomized and matrix-free direct solvers for large structured dense linear systems*, SIAM J. Sci. Comput., 38 (2016), pp. S508–S538.
- 600 [24] P. G. MARTINSSON, *A fast randomized algorithm for computing a hierarchically semiseparable representation of a matrix*, SIAM J. Matrix Anal. Appl., 32 (2011), pp. 1251–1274.
- 601 [25] P. G. MARTINSSON AND V. ROKHLIN, *An accelerated kernel-independent fast multipole method in one dimension*, SIAM J. Sci. Comput., 29 (2007), pp. 1160–1178.
- 602 [26] P. G., MARTINSSON, V. ROKHLIN, AND M. TYGERT, *A fast algorithm for the inversion of general Toeplitz matrices*, Comput. Math. Appl., 50 (2005), pp. 741–752.
- 603 [27] X. OU AND J. XIA, *A stable matrix version of the fast multipole method: the 2D version with stability analysis*, preprint.
- 604 [28] X. OU AND J. XIA, *SuperDC: Stable superfast divide-and-conquer eigenvalue decomposition*, submitted, (2021), arXiv:2108.04209.

632 [29] V. ROKHLIN, *Rapid solution of integral equations of classical potential theory*, J. Comput. Phys., 60 (1985),
 633 pp. 187–207.

634 [30] F. H. ROUET, X. S. LI, P. GHYSELS, AND A. NAPOV, *A distributed-memory package for dense hierarchically*
 635 *semi-separable matrix computations using randomization*, ACM Trans. Math. Software, 42 (2016), pp.
 636 1–35.

637 [31] J. SHEN, Y. WANG, AND J. XIA, *Fast structured direct spectral methods for differential equations with*
 638 *variable coefficients. I. The one-dimensional case*, SIAM J. Sci. Comput., 38 (2016), pp. A28–A54.

639 [32] X. SUN AND N. P. PITTSIANIS, *A matrix version of the fast multipole method*, SIAM Rev., 43 (2001),
 640 pp. 289–300.

641 [33] J. VOGEL, J. XIA, S. CAULEY, AND V. BALAKRISHNAN, *Superfast divide-and-conquer method and pertur-*
 642 *bation analysis for structured eigenvalue solutions*, SIAM J. Sci. Comput., 38 (2016), pp. A1358–A1382.

643 [34] Y. XI AND J. XIA, *On the stability of some hierarchical rank structured matrix algorithms*, SIAM J. Matrix
 644 Anal. Appl., 37 (2016), pp. 1279–1303.

645 [35] Y. XI, J. XIA, S. CAULEY, AND V. BALAKRISHNAN, *Superfast and stable structured solvers for Toeplitz*
 646 *least squares via randomized sampling*, SIAM J. Matrix Anal. Appl., 35 (2014), pp. 44–72.

647 [36] J. XIA, *Fast Direct Solvers for Structured Linear Systems of Equations*, Ph.D. Thesis, University of California,
 648 Berkeley, 2006.

649 [37] J. XIA, *On the complexity of some hierarchical structured matrix algorithms*, SIAM J. Matrix Anal. Appl., 33
 650 (2012), pp. 388–410.

651 [38] J. XIA, S. CHANDRASEKARAN, M. GU, AND X.S. LI, *Fast algorithms for hierarchically semiseparable*
 652 *matrices*, Numer. Linear Algebra Appl., 17 (2010), pp. 953–976.

653 [39] J. XIA, Y. XI, AND M. GU, *A superfast structured solver for Toeplitz linear systems via randomized sampling*,
 654 SIAM J. Matrix Anal. Appl., 33 (2012), pp. 837–858.

655 [40] N. YARVIN AND V. ROKHLIN, *A generalized one-dimensional fast multipole method with application to*
 656 *filtering of spherical harmonics*, J. Comput. Phys., 147 (1998), pp. 594–609.

657 [41] X. YE, J. XIA, AND L. YING, *Analytical low-rank compression via proxy point selection*, SIAM J. Matrix
 658 Anal. Appl., 41 (2020), pp. 1059–1085.

659 [42] L. YING, *A kernel independent fast multipole algorithm for radial basis functions*, J. Comput. Phys., 213
 660 (2006), pp. 451–457.

661 [43] L. YING, G. BIROS, AND D. ZORIN, *A kernel-independent adaptive fast multipole algorithm in two and three*
 662 *dimensions*, J. Comput. Phys., 196 (2004), pp. 591–626.